



Stepwise model parametrisation using satellite imagery and hemispherical photography: Tuning AquaCrop sensitive parameters for improved winter wheat yield predictions in semi-arid regions

Bader Oulaid^{a,b,c,*}, Alice E. Milne^b, Toby Waine^a, Rafiq El Alami^c, Maryam Rafiqi^c, Ron Corstanje^a

^a Cranfield University, College Road, Cranfield, Bedford MK43 0AL, United Kingdom

^b Net-Zero and Resilient Farming, Rothamsted Research, Harpenden, Hertfordshire AL5 2JQ, United Kingdom

^c Mohammed VI Polytechnic University, Lot 660, Moulay Rachid, Ben Guerir 43150, Morocco

ARTICLE INFO

Keywords:

Crop modelling
Canopy cover
Wheat yield
Model performance
Soil fertility modelling

ABSTRACT

Crop models are complex with many parameters, which has limited their application. Here we present an approach which both removes the model complexity through reducing the parameter dimensionality through sensitivity analysis, and presents a subsequent efficient approach to model parameterisation using swarm optimisation. We do this for two key model outputs, crop canopy and yield, and for two types of observational data, hemispheric photographs and Landsat7 imagery. Importantly we compare the usefulness of these two sources of data in terms of accurate yield prediction. The results showed that the dominant model parameters that predict canopy cover were generally consistent across the fields, with the exception of those related water stress. Although mid-season canopy cover extracted from Landsat7 was underestimated, good agreement was found between the simulated and observed canopy cover for both sources of data. Subsequently, less accurate yield predictions were achieved with the Landsat7 compared to the hemispherical photography-based parametrizations. Despite the small differences in the canopy predictions, the implications for yield prediction were substantial with the parametrization based on hemispherical photography providing far more accurate estimates of yield. There are, however, additional resource implications associated with hemispherical photography. We evaluate these trade-offs, providing model parametrization sets and demonstrating the potential of satellite imagery to assist AquaCrop, particularly on large scales where ground measurements are challenging.

1. Introduction

Crop growth models use empirical and mathematical relationships to simulate the growth and development of crops under diverse conditions, making them important tools to inform agricultural decisions (Soltani et al., 2020). Several crop growth models have been successfully used to assist sustainable crop production including DSSAT (Ngwira et al., 2014), CROPWAT (Tsakmakis et al., 2018) and APSIM (Zhang et al., 2022a). While these models are effective in simulating yield under various management practices (Choruma et al., 2021; Jing et al., 2021; Zhang et al., 2022b), their broader use has been restricted due to their complexity: they need a relatively large number of input parameters, most of which are difficult to obtain in practice. Given this complexity, the FAO devised a simple and resilient model, AquaCrop (Raes et al., 2009), which requires a smaller number of intuitive input parameters.

This model has been used in many studies to predict yield and irrigation requirements (Khabba et al., 2020; Wang et al., 2022) and has also been tested to be effective for a wide variety of crops, such as wheat (Toumi et al., 2016a, 2016b), potato (Razzaghi et al., 2017; Wale et al., 2022), sunflower (Stricevic et al., 2011), tomato (Takács et al., 2021), maize (Greaves and Wang, 2016), and table grape (Er-Raki et al., 2021). According to the findings of all these studies, the AquaCrop model is able to reliably simulate responses to a variety of field management practices.

The usefulness of process-based models like AquaCrop is usually constrained by the fact that they are often calibrated for a specific circumstance and so may not be transferable to other case studies. For example, Paredes et al. (2015) found that uncalibrated, the AquaCrop model was unable to accurately forecast the yield and the biomass of soybeans in North China Plain since there was a noticeable tendency for under-estimation for both predictions with deviations of more than 27%

* Corresponding author at: Net-Zero and Resilient Farming, Rothamsted Research, Harpenden, Hertfordshire AL5 2JQ, United Kingdom.

E-mail address: bader.oulaid@rothamsted.ac.uk (B. Oulaid).

<https://doi.org/10.1016/j.fcr.2024.109327>

Received 18 May 2023; Received in revised form 21 February 2024; Accepted 27 February 2024

Available online 8 March 2024

0378-4290/© 2024 The Authors. Published by Elsevier B.V. This is an open access article under the CC BY-NC license (<http://creativecommons.org/licenses/by-nc/4.0/>).

and 20%, respectively. Thus, areas where the model may be used can be expanded only by calibrating it across many sites with various sowing dates, seeding rates, fertilization programmes, and irrigation programmes. Given that AquaCrop is well suited for modelling crop production and that AquaCrop is widely used in Morocco (Benabdelouahab et al., 2016), the creation of calibrated regional parameterization would be advantageous.

A number of approaches have been used to calibrate the AquaCrop for a specific area. Most of these studies estimate the parameters by matching phenological observations to certain parameters and adopting default values for others (Abi Saab et al., 2021; Dirwai et al., 2021; Lu et al., 2021). In many cases the observational field data was used to parameterize AquaCrop through a process of trial-and-error where data comes from several plots or fields and then the mean of the parameter values is used (Toumi et al. (2016a),(2016b)). This provides a simple but pragmatic approach to calibration. More generally, process model parameterisation has been explored by a number of authors. The first step is often to use a sensitivity analysis to identify which parameters most influence the outcome of interest; these then become the focus of the parameterisation. Sensitivity analysis includes evaluating the local and global influence of individual parameters or combinations thereof. Local sensitivity analysis facilitates identifying parameters that have a direct effect on model predictions by examining the effect of minor changes in a single parameter on the model output. In contrast, global sensitivity analysis takes into consideration interactions and non-linear effects. Techniques such as Sobol indices (Nossent et al., 2011; Vazquez-Cruz et al., 2014; Xing et al., 2017a), Morris method (Morris, 1991a; Paleari et al., 2021; Specka et al., 2015), and FAST (McRae et al., 1982; Xu and Gertner, 2011) are frequently adopted. Building on the insights gained from sensitivity analysis, the next step is model parameterization. The advancement in parameterization techniques for crop growth models covers forcing, calibration, and updating methods, each contributing to the refinement and reliability of model predictions (Jin et al., 2018). Forcing methods leverage remote sensing and field measured data using algorithms like linear interpolation (Dhillon et al., 2020; Pelosi et al., 2022) and wavelet methods (Hariharan and Kannan, 2014; Krishnan et al., 2023) to substitute missing or incomplete crop model simulations with information derived from observed or remotely sensed sources. Findings from Casa et al. (2012) and Morel et al. (2014) highlight the effectiveness of forcing techniques in overcoming limitations related to the lack of detailed knowledge about management practices or soil characteristics. Calibration involves comparing the model's predictions or simulations to observed data and then adjusting the model parameters or inputs to reduce discrepancies between the model output and actual observations. Calibration is often performed using optimization techniques to find the best combination of parameter values that minimizes the difference between model predictions and observed data (Jin et al., 2016; Lyu et al., 2022). For example, Li et al. (2018) coupled the GLUE method and experimental field data to parametrise DSSAT-CERES model, the method showcased its accuracy in estimating wheat genotype parameters. Dong et al. (2013) introduced a VFSA optimization algorithm for LAI assimilation into the CERES-Wheat model, and demonstrated an improved accuracy, especially for LAI in winter wheat experiments. Lastly, updating methods refer to techniques that integrate observational data into the model to improve its accuracy and reliability. The goal is to adjust the model's predictions in light of real-world observations, making it more consistent with the observed behaviour of the system. In the context of crop modelling, data assimilation can be used to repeatedly update crop model simulations, for example, when remote sensing data is available. Zhang et al. (2022) developed an ensemble Kalman filter (EnKF) data assimilation framework to assimilate plant and soil observations into the APSIM-Wheat model, and the results showed an improvement in crop development and yield simulations. In this paper we are concerned with calibration using optimisation.

There are two key considerations for obtaining a parameterised model for any given circumstance or case study; i) data, in the form of

observations, are needed for the key variables of interest (canopy cover and yield) across the growing season and once obtained, ii) an efficient optimisation procedure which is capable of considering the full model parameter space conditional to the particularities of study areas of interest. One method for obtaining canopy cover measurements is through hemispherical handheld photography. The technique is based on a determination of how much sky is visible through the canopy, by categorising each pixel of the image as either belonging to the sky or to any plant obstructing object. Although this approach offers a direct way to assess canopy cover, it is labour-intensive, time-consuming, and requires specialised equipment. Remote sensing offers an alternative means of predicting canopy cover directly using dedicated software such as *Sen2r* (Ranghetti et al., 2020), or indirectly through vegetation indices (VIs). While remote sensing provides a cost-free method for estimating canopy cover expansion across multiple time and space scales, it is often affected by limiting factors, such as sensor failures and/or cloud cover obscuring satellite imagery.

There are many optimization algorithms available, and these can be generally characterized as either local or global optimizations. Local methods use an iterative search beginning with the nominal value of the parameter but can become trapped in a local minimum and prematurely terminate the search (Poempool et al., 2018). Global optimization searches adopt mechanism to search a larger part of the search space and are more frequently used to parameterize crop models. Here, methods include particle swarm optimization (Kennedy and Eberhart, 1995), the fast simulated annealing (Szu and Hartley, 1987), and the Artificial bee colony (Akbari et al., 2010). Particle swarm optimization (PSO) has recently increased in popularity and has been used in a variety of applications, including the enhancement of crop yield estimate accuracy (Sabzadeh and Shourian, 2020), and the assimilation of remotely sensed data into decision support systems (Wagner et al., 2020). It is appealing because of its ease of implementation and ability to quickly converge to a reasonably good solution compared to classic optimization algorithms, which have great search capability but poor convergence speed and computing efficiency (Xu and Yu, 2018).

This study presents a methodological framework to determine case specific crop model parameterization. We use the Morris and FAST methods as preliminary steps to analyse the impact of different parameters on AquaCrop key responses, including canopy cover aboveground biomass, and yield. A key novelty here is that we assess the utility of canopy cover estimates obtained from two distinct sources (i.e., Landsat 7 satellite imagery and hemispherical photographs) for calibrating the AquaCrop canopy simulation. Unlike traditional calibration methods reliant on trial and error, our approach is a stepwise automatic parameterisation. In support of our framework, we enhanced the Matlab implementation of AquaCrop by incorporating a soil fertility component. We demonstrated our framework for a semi-arid region in Morocco.

2. Material and methods

2.1. Aquacrop model

AquaCrop is a multi-crop water driven model that evolved from the FAO Irrigation Drainage Paper 33 (Doorenbos et al., 1979). The model avoids the confounding effect of non-productive water consumption by separating the actual evapotranspiration (ET) into crop transpiration (Tr) and soil evaporation (E). AquaCrop uses a comparatively small number of parameters to assess the effect of environment and management practices on crop growth. The final crop yield is estimated through four steps: i) simulate the foliage development represented by the green canopy cover (CC); ii) calculate the crop transpiration (Tr) using the reference evapotranspiration (ET_0) and the crop coefficient; iii) produce the above-ground biomass (B) as a function of the cumulative amount of water transpired; and (iv) simulate the final crop yield by multiplying biomass (B) with a Harvest Index (HI). Details can be found

in Raes et al. (2009) and Steduto et al. (2009). In this study, the MATLAB version of the AquaCrop model (AquaCrop-OS) developed by Foster et al. (2017) which is available at (www.aquacropos.com) was used. The soil fertility feature is not implemented in AquaCrop AOS v6.0a. Based on AquaCrop reference manual (Steduto et al., 2009), a code to account for the influence of soil fertility on canopy cover growth (KS_{CGC}), maximum canopy cover (KS_{CCX}), and biomass water productivity (KS_{WP^*}) was integrated to AquaCrop as defined in Eqs. 1, 2 and 3 respectively.

$$KS_{CGC} = \frac{e^{S_{rel}f_{CGC}} - 1}{e^{f_{CGC}} - 1} \quad (1)$$

$$KS_{CCX} = \frac{e^{S_{rel}f_{CCX}} - 1}{e^{f_{CCX}} - 1} \quad (2)$$

$$KS_{WP^*} = \frac{e^{S_{rel}f_{WP^*}} - 1}{e^{f_{WP^*}} - 1} \quad (3)$$

where S_{rel} is the relative stress level in the studied fields. The coefficients f_{CGC} , f_{CCX} and f_{WP^*} are the shape factors describing the effects of soil fertility on canopy growth, maximum canopy cover and biomass water productivity, respectively.

2.2. Study and data description

2.2.1. Study site

Field experiments were conducted at an irrigated zone of the Haouz plain during two successive growing seasons: 2002–2003 and 2003–2004 by Toumi et al. (2016a),(2016b). The area is located 40 km east of Marrakech (Fig. 1). In season 2002–2003, three field were investigated (we refer to these as A1, A2 and A3) and in season 2003–2004, six fields were investigated (referred hereafter as B1, B2, B3, B4, B5 and B6). In this area, the irrigation scheduling is managed by ORMVAH (Office Regional de Mise en Valeur Agricole du Haouz), a

regional agricultural advisory body for the management of hydro-agricultural equipment and water resources for agricultural use. The region's climate is characterized as semi-Mediterranean with an average annual precipitation of about 240 mm falling between November and May.

The red parcels are from season 2003–2004 and the grey parcels are related to 2002–2003 growing season.

2.2.2. Data description

AquaCrop requires daily measurements of maximum and minimum temperatures, precipitation, and reference evapotranspiration as weather input variables. We sourced Weather data from Agafay weather stations (31.47 °N, 8.21 °W). The maximum and minimum air temperatures in 2002–2003 were 38.1 and -0.4 °C respectively while the comparative temperatures were 38.4 and -2.04 °C in 2003–2004 (for more details see Appendix A, Fig. A.1). Data collected from the studied fields included canopy cover (CC), aboveground biomass and yield values. Canopy cover was measured using hemispherical canopy photographs for two seasons: Each field was differently managed in terms of sowing date and irrigation schedule. Details are given in Table 1.

For model calibration and validation, we required data on canopy cover and yield. We used two approaches to estimate our first state variable (CC). In the first method, the canopy cover of our calibration sites was measured over the growing season using hemispherical canopy images taken with a Nikon Coolpix 950 and FC-E8 fish-eye lens converter with a field of view of 183 degrees by Toumi et al. (2016a), (2016b). Following image acquisition, the CAN eye software was used for image analysis. In the pre-processing stage, all images were converted to grayscale, using 256 levels of intensity, and then transformed into binary format to distinguish between black and white pixels. Subsequently, the image with the optimal contrast between the canopy and the sky was selected. This selection process aimed to identify the image with the least number of saturated pixels, ensuring the best representation of the canopy-sky interface. The images were then classified into

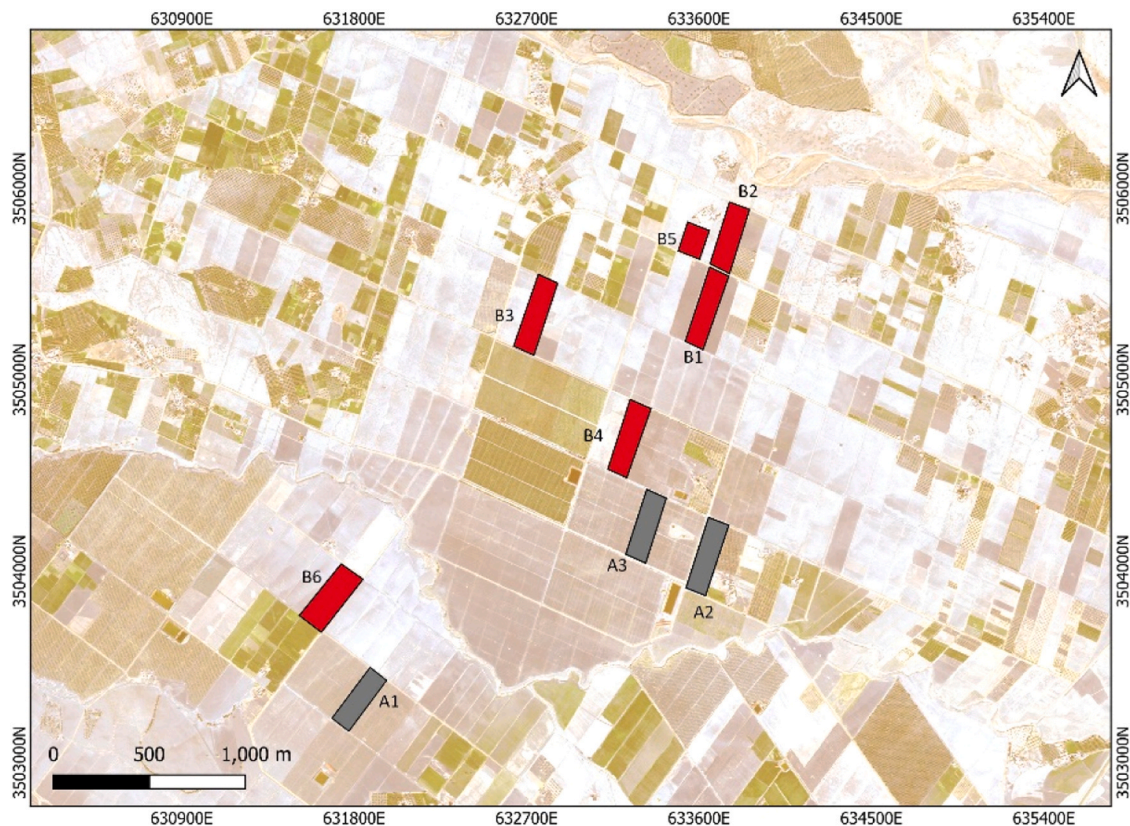


Fig. 1. Location of the study area showing the study fields in which irrigated wheat was grown.

Table 1

Sowing and irrigation schedule for the studied fields (taken from Toumi et al. 2016a,2016b). Fields A1, A2, A3 were irrigated with 30 mm per event, while fields B1, B2, B3, B4, B5, B6 received 60 mm per irrigation event.

Parcel ID	Sowing dates	Irrigation dates						Total irrigation amount (mm)
		1st	2nd	3rd	4th	5th	6th	
A1	17th December 2002	28th January 2003	22nd February 2003	10th April 2003				90
A2	11th January 2003	01st February 2003	21st February 2003	14th March 2003	24th March 2003	07th April 2003	24th April 2003	180
A3	14th January 2003	04th February 2003	20th February 2003	14th April 2003	21st April 2003			120
B1	21st November 2003	20th January 2004	23rd February 2004	01st April 2004				180
B2	21st November 2003	16th January 2004	17th February 2004	28th March 2004				180
B3	15th December 2003	20th January 2004	15th February 2004	17th March 2004				180
B4	19th December 2003	18th January 2004	24th February 2004	21st April 2004				180
B5	20th December 2003	16th January 2004	16th February 2004	26th March 2004				180
B6	24th December 2003	26th January 2004	21st February 2004	27th March 2004				180

Table 2

Landsat 7 band specifications.

Band	Spatial resolution (m)	Wavelength (µm)	Description
B1	30	0.45 – 0.52	Blue
B2	30	0.52 – 0.60	Green
B3	30	0.63 – 0.69	Red
B4	30	0.77 – 0.90	Near infrared (NIR)
B5	30	1.55 – 1.75	Shortwave infrared 1 (SWIR1)
B6	60	10.40 – 12.50	Thermal infrared (TIR)
B7	30	2.08 – 2.35	Shortwave infrared 2 (SWIR2)

black and white bitmaps using the CAN EYE software and canopy cover was expressed as percentages. More details about this process are provided by Khabba et al. (2009). In the second approach, free atmospherically corrected satellite imagery was extracted from the Landsat7 ETM+ sensor and processed it using GEE Python API (Gorelick et al., 2017) to calculate the normalized difference vegetation index (NDVI). Landsat 7 provides medium spatial resolution of 30 m images with a revisit time of 16 days. The image collections are created with the Landsat Ecosystem Disturbance Adaptive Processing System (LEDAPS) algorithm (Schmidt et al., 2013) and contain 4 visible bands (blue, green, red and near infrared), two short-wave infrared bands (SWIR1, SWIR2) and one thermal infrared band (TIR) as shown in Table 2.

The automated workflow for computation of the NDVI started with an extraction of an image collection covering the crop growth cycle of our calibration sites. A bitmask band was used to mask pixels that contain cirrus and high clouds, then a buffer of 30 m was applied to avoid the edges that mislead the calculation of NDVI values (Vannoppen and Gobin, 2021).

We used the formula by Tenreiro et al. (2021) to estimate canopy cover from Normalized Difference Vegetation Index (NDVI). Tenreiro et al. (2021) derived the formula from a meta-analysis incorporating data from 19 studies, including the significant study conducted by Er-raki et al. (2007) focusing on the Tensift Al Haouz region and aligns with our study area. The derived formula, specifically tailored for wheat and exhibits a statistically significant fit and reasonable accuracy, as evidenced by an R-squared value of 0.71 and an RMSE of 14.2. Both coefficients in the model have been verified to be statistically significant at the 5% level, providing robustness to the derived equation.

$$CC = 97.368NDVI - 4.942 \tag{4}$$

Table 3

Average aboveground biomass and yield in the study area with the range of measured values given in brackets.

Season	2002–2003			2003–2004					
	A1	A2	A3	B1	B2	B3	B4	B5	B6
Biomass (t ha ⁻¹)	6.02	4.58	1.97	6.5	4.85	5.04	6.67	2.91	5.01
	[5.6–6.3]	[4.2–5.2]	[1.5–2.2]	[6.2–7]	[4.5–5.3]	[4.7–5.3]	[6.4–6.9]	[2.5–3.2]	[4.7–5.2]
Yield (t ha ⁻¹)	2.76	2.09	0.9	2.99	2.23	2.29	3.26	1.32	2.26
	[2.5–3]	[1.8–2.2]	[0.7–1]	[2.5–3]	[2–2.5]	[2–2.5]	[3–3.5]	[1–1.5]	[2–2.5]

We refer to these measures of CC as referred hereafter as CC_{L7}. To estimate grain yield, plants were sampled from five quadrates of size 0.5 m×0.5 m selected randomly from across the field. From each quadrate, subsamples of plants were selected at random, and the number and weight of grains were measured (Table 3).

2.3. Sensitivity analysis methods

2.3.1. Morris

Morris (1991b) established the elementary effects method, which was further refined by Campolongo et al. (2007), to determine the model parameters (and their interactions) that most influences the output of interest. This method is suitable for models with a large number of parameters. For a model with *k* independent inputs. The input space (Ω) is discretized into a number of equal segments of size Δ . The *i*th input factor's elementary effect is defined as:

$$EE_i = \frac{[Y(X_1, X_2, \dots, X_{i-1}, X_i + \Delta, \dots, X_k) - Y(X_1, X_2, \dots, X_k)]}{\Delta} \tag{5}$$

As a result, each EE_i is a measure of the local variation of the model response *Y* in response to a change in the related model parameter. The Elementary effects distribution F_i is determined for the *i*th input factor by randomly sampling different parameters (*X*) from Ω . Morris' approach computes two sensitivity measures: the mean (μ) and the standard deviation (σ) of the sensitivity measure. A significant standard deviation σ indicates that the input has a nonlinear effect or interacts with other inputs, while large μ indicates that the overall effect of that input on the output is greater. Certain effects may cancel out when calculating μ , resulting in a low mean value for even a significant component. To prevent such Type II errors, Campolongo et al. (2007) advocated substituting μ^* for μ , which is defined as an estimate of the mean of the distribution of the elementary effects' absolute values. Morris' measures for the *i*th input are defined as:

$$\mu_i = \frac{1}{r} \sum_{j=1}^r EE_i^j \tag{6}$$

$$\sigma_i^2 = \frac{1}{r-1} \sum_{j=1}^r (EE_i^j - \mu)^2 \tag{7}$$

$$\mu_i^* = \frac{1}{r} \sum_{j=1}^r |EE_i^j| \tag{8}$$

Where r is the number of trajectories constructed from the sampling of X from Ω and EE_i^j indicates the elementary effects relative to the i^{th} factor computed along trajectory j .

A qualitative parameter ranking based on the Morris technique was established as the first step of the AquaCrop model's SA. Morris analysis samples were generated within the defined sample using the Latin Hypercube sampling design. In practice, the number of trajectories r should be as large as possible, as larger trajectories values provide a more complete coverage of the parameter space and a lower uncertainty associated with the estimated sensitivity indices (Ćiric et al., 2012). $r = 50$ trajectories was applied, which is the maximum value suggested by Campolongo et al. (2007) to guarantee a high coverage of the input space. When all 36 model parameters were evaluated, a total of 50 trajectories needed a maximum of $n = 1850$ model evaluations.

2.3.2. Fourier Amplitude Sensitivity Test (FAST)

First-order sensitivity indices measure the variance created by a

single parameter in variance-based methods. Cukier et al. (1973) developed the Classical FAST method. FAST samples the input parameter space with a transformation function. The transformation function for FAST sampling is defined as:

$$x_i = (0.5 + \frac{1}{\pi}[\arcsin[\sin(w_i s + \rho_i)]])k_i \tag{9}$$

where x_i is the i th parameter, s is the sampling range with $s \in [-\pi, \pi]$, ρ_i is a random phase shift parameter marking the starting point of the search curve, $\rho_i \in [0, 2\pi]$, w_i ($i = 1, \dots, k$) is the individual assigned integer frequency of parameter x_i , and k_i is a scaling factor to scale the value of the transformation function that lies between 0 and 1 to the appropriate parameter range. Since the transformation function is periodic, a sampling range of 2π is sufficient for decomposition. The first-order sensitivity indices (S_i) describe the major effects of parameters by calculating how the input variance contributes to the overall output variance. Saltelli et al. (1999) improved the FAST approach to generate first order

Table 4

List of the parameters from AquaCrop that were investigated in the sensitivity analysis with published lower and upper bounds where available and associated references.

Name	Definition	Unit	Lower bound	Upper bound	References
Input parameters					
gEme	Time from sowing/transplanting to emergence	Days/GDD's	63	114	Toumi et al. (2016a), (2016b)
gZx	Time from sowing/transplanting to maximum root development	Days/GDD's	484	616	Iqbal et al. (2014)
gYld	Time from sowing/transplanting to start of yield formation	Days/GDD's	600	780	^a
gSen	Time from sowing/transplanting to start of canopy senescence	Days/GDD's	800	1000	-
gMat	Time from sowing/transplanting to physiological maturity	Days/GDD's	1400	1500	-
gFlwDur	Duration of flowering	Days/GDD's	100	200	Vanuytrecht et al. (2014)
gYldDur	Duration of yield formation	Days/GDD's	300	600	-
CCX	Maximum fractional canopy cover size	-	0.73	0.99	-
CDC	Canopy decline coefficient	GDD/day	0.004	0.0067	-
CGC	Canopy growth coefficient	GDD/day	0.005	0.0093	-
Zn	Minimum effective rooting depth	Metres	0.1	0.39	Toumi et al. (2016a), (2016b)
Zx	Maximum effective rooting depth	Metres	0.55	2.4	Toumi et al. (2016a), (2016b)
sZsp	Shape factor describing the decreasing speed of root expansion over time	-	10	19	Xing et al. (2017)
WxTopZ	Maximum water extraction at the top of the root zone	$m^3 m^{-3} day^{-1}$	0.0189	0.048	Xing et al. (2017)
WxBotZ	Maximum water extraction at the bottom of the root zone	$m^3 m^{-3} day^{-1}$	0.0056	0.012	Vanuytrecht et al. (2014)
cdAge	Decline of crop coefficient due to ageing of the canopy	$\% day^{-1}$	0.21	0.39	Xing et al. (2017)
Kcb	Maximum crop coefficient when canopy is fully developed	-	0.77	1.43	Xing et al. (2017)
Wp	Water productivity normalised for reference evapotranspiration and atmospheric carbon dioxide	g/m^2	11	22	Xing et al. (2017)
Wpy	Adjustment of water productivity parameter in yield formation stage	% of WP	75	125	Silvestro et al. (2017)
Hi0	Reference harvest index	-	0.32	0.61	Xing et al. (2017)
exF	Excess of potential fruits that is produced by the crop	%	70	130	Xing et al. (2017)
Output responses					
dxHi0	Maximum possible increase in harvest index above reference value	%	10	19	Xing et al. (2017)
gMnB	Minimum number of GDD's required for full biomass production	GDD's	13	15	-
Aer	Water deficit below saturation at which aeration stress begins to occur	%	3.5	6.5	Xing et al. (2017)
pExpUp	Upper soil water depletion threshold for water stress effects on canopy expansion	-	0.14	0.26	Upreti et al. (2020)
pStmUp	Upper soil water depletion threshold for water stress effects on stomatal control	-	0.455	0.845	Upreti et al. (2020)
pSenUp	Upper soil water depletion threshold for water stress effects on canopy senescence	-	0.49	0.91	Upreti et al. (2020)
pPolUp	Upper soil water depletion threshold for water stress effects on crop pollination	-	0.455	1	Upreti et al. (2020)
pExpLo	Lower soil water depletion threshold for water stress effects on canopy expansion	-	0.445	0.845	Upreti et al. (2020)
pStmLo	Lower soil water depletion threshold for water stress effects on stomatal control	-	0.7	1	Upreti et al. (2020)
pSenLo	Lower soil water depletion threshold for water stress effects on canopy senescence	-	0.7	1	Upreti et al. (2020)
pPolLo	Lower soil water depletion threshold for water stress effects on crop pollination	-	0.7	1	Upreti et al. (2020)
sExp	Shape factor describing water stress effects on canopy expansion	-	2.1	3.9	Upreti et al. (2020)
sStm	Shape factor describing water stress effects on stomatal control	-	1.75	3.25	Upreti et al. (2020)
sSen	Shape factor describing water stress effects on canopy senescence	-	2.1	3.9	Upreti et al. (2020)
sPol	Shape factor describing water stress effects on crop pollination	-	0.7	1.3	Upreti et al. (2020)
Cc	Fractional canopy cover	-	-	-	-
Bio	Accumulated aboveground biomass	Kg/ha	-	-	-
Yield	Crop yield	ton/ha	-	-	-

^a These bounds were adjusted from the literature values to account for the fact we used a based temperature of 5 °C (which is often adopted for Wheat grown in Northern Africa) as opposed to the more standard base temperature of 0 °C.

(S_i) and total sensitivity indices (TS_i) named Extended FAST that does not only account for an input's variability but also the variance caused by other parameters. While there is no broad agreement on the appropriate cut-off value for parameter significance, first-order index value of 0.01 is commonly used to differentiate sensitive from insensitive parameters, i.e. parameters with smaller indices than 0.01 contribute less than 1% of the variation in the output and are thus deemed non-influential.

2.3.3. Sensitivity analysis strategy

A total of 36 AquaCrop parameters (Table 4) were identified as relevant for the calibration of the canopy cover, biomass, and yield predictions. The literature was reviewed to identify plausible ranges of the model parameters, then Morris method was used to screen out parameters with marginal effects and to identify a subset of relevant model parameters. Finally, the Fourier Amplitude Sensitivity Test (FAST) method was implemented to quantify both the first and higher order parameter sensitivities on above ground biomass (AGB), canopy cover (CC) and yield for wheat crops in the nine study fields. The sensitivity analysis was implemented in MATLAB (MathWorks Inc., 2020).

2.4. Stepwise model parameter optimization

Parcels A1 – A3 were used to calibrate the model and parcels B1 – B6 served as our validation set. A two-step calibration approach was adopted by first fitting the canopy cover and then the yield. Both steps use particle swarm optimization. Each optimization phase fits only the parameters that were found to be relevant for that phase in the sensitivity analysis. The PSO optimization started by randomly allocating the initial position and velocity of the optimizer. Parameters were allowed to take values within a range not exceeding 20% of the lower and upper bounds we found in the literature (see Table 4). Then, an executable MATLAB file was run to simulate the canopy cover from input data including weather, soil, crop, and management data and taking into account the effect of soil fertility stress on both canopy cover and yield outputs. The optimization searches the parameter space aiming to

minimize the objective function which we defined as the sum of squared differences between the observed and simulated measures.

For the canopy cover fitting, we used two objective functions, one using the CC_{HP_i} canopy estimates and the other using CC_{L7_i} . The constructed objective functions are given by:

$$J_{HP} = \sum_{j=1}^p \sum_{i=1}^n (CC_{S_i} - CC_{HP_i})^2 \tag{10}$$

$$J_{L7} = \sum_{j=1}^p \sum_{i=1}^n (CC_{S_i} - CC_{L7_i})^2 \tag{11}$$

where n is the number of measurements, p is the number of calibration sites, CC_{S_i} is the simulated canopy cover, CC_{HP_i} and CC_{L7_i} are the estimated canopy cover using the hemispherical photographs and Landsat7, respectively. We then took each of these parameter sets forward to the second stage of yield fitting where our objective functions were the sum of squared differences between model and measured yield. This resulted in two sets of model parameters. The stepwise model parameterization deliberately excluded biomass fitting as our objective was to create an easily transferable and resource-efficient approach. Recognizing the challenges associated with obtaining accurate biomass measurements, the focus was placed on canopy cover (CC) data from diverse sources, such as hemispherical photographs (HP) and Landsat 7 (L7). A comprehensive conceptual framework illustrating the described methodology is presented in Fig. 2.

2.5. Model evaluation

The performance of each parameter set was evaluated by predicting the responses for the six validation fields (B1, B2, B3, B4, B5 and B6) and then calculating four performance metrics. These were the coefficient of determination (R^2) which expresses the degree of collinearity between the observed and simulated data, the normalized root mean square error (NRMSE), the Nash and Sutcliffe modelling efficiency (EF) as a model performance indicator (Nash and Sutcliffe, 1970) and the Willmott's

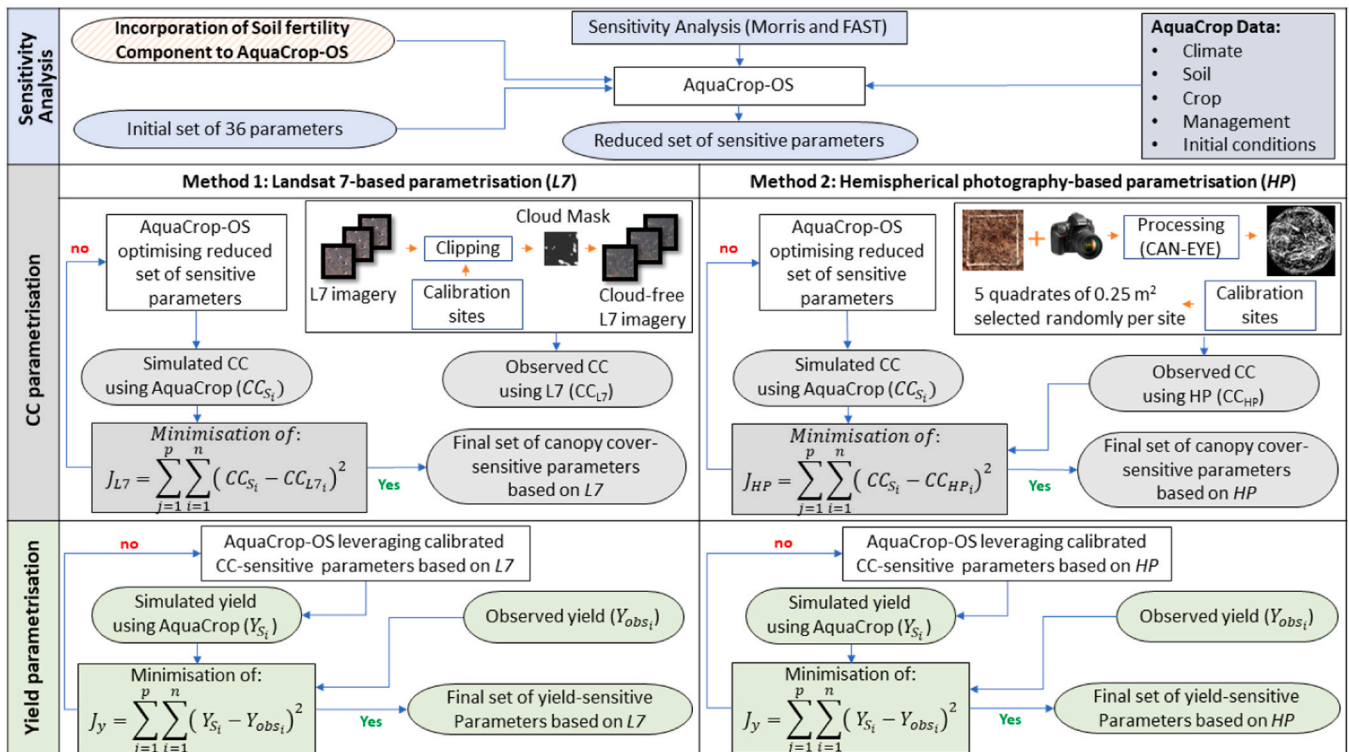


Fig. 2. Conceptual framework of the sensitivity analysis and the stepwise parametrisation of AquaCrop.

Table 5

The rank order of the mean of elementary effects (μ^*) for the Morris sensitivity analysis. Increasing ranks imply reduced sensitivity with the parameter ranked one the most sensitive (See Table 4 for definitions).

Output response	Input parameters ^a	Parcels									
		A1	A2	A3	B1	B2	B3	B4	B5	B6	
Yield	Wp	1	1	1	1	1	1	1	1	4	
	Hi0	2	2	2	2	2	2	2	2	5	
	gYld	3	5	^b	-	-	-	-	-	1	
	CGC	4	4	4	5	4	4	4	3	-	
	pExpLo	5	3	3	-	-	3	3	4	-	
	Kcb	-	-	5	3	3	5	5	5	-	
	Wpy	-	-	-	4	5	-	-	-	-	
	gEme	-	-	-	-	-	-	-	-	2	
	pStmLo	-	-	-	-	-	-	-	-	3	
	Biomass	Wp	1	3	3	1	1	1	2	1	1
CGC		2	2	4	3	3	3	3	3	4	
CDC		5	-	-	4	4	-	-	4	-	
Kcb		4	4	-	2	2	5	5	5	5	
WxBotZ		-	-	-	-	-	4	4	-	3	
WxTopZ		-	5	1	-	-	-	-	-	-	
pSenUp		-	-	5	-	-	-	-	-	-	
gSen		-	-	-	5	5	-	-	-	-	
pExpLo		3	1	2	-	-	2	1	2	2	
CDC		2	1	4	1	1	2	2	1	-	
Canopy cover	gSen	4	5	-	2	2	1	5	4	-	
	gMat	3	4	2	4	4	-	3	3	5	
	gEme	-	-	-	-	-	-	-	-	1	
	CCX	-	-	-	5	-	-	-	-	-	
	Zx	5	-	-	3	3	5	1	2	-	
	WxTopZ	1	2	1	-	-	3	4	5	4	
	WxBotZ	-	3	3	-	-	4	-	-	-	
	pExpLo	-	-	5	-	-	-	-	-	-	
	pStmLo	-	-	-	-	-	-	-	-	2	
	pStmUp	-	-	-	-	-	-	-	-	3	
Zn	-	-	-	-	5	-	-	-	-		

^a Most sensitive parameters for all parcels.

^b parameter is not ranked among the five most sensitive parameters.

index of agreement (D-index). These are defined as follows:

$$R^2 = \left(\frac{\sum_{i=1}^n (O_i - \bar{O})(P_i - \bar{P})}{\sqrt{\sum_{i=1}^n (O_i - \bar{O})^2} \sqrt{\sum_{i=1}^n (P_i - \bar{P})^2}} \right)^2 \quad \# \quad (12)$$

$$NRMSE = \frac{100}{\bar{O}} \left[\frac{\sum_{i=1}^n (P_i - O_i)^2}{n} \right]^{0.5} \quad \# \quad (13)$$

$$EF = 1 - \frac{\sum_{i=1}^n (O_i - P_i)^2}{\sum_{i=1}^n (O_i - \bar{O})^2} \quad \# \quad (14)$$

$$D - index = 1 - \frac{\sum_{i=1}^n (P_i - O_i)^2}{\sum_{i=1}^n (|P_i - \bar{O}| + |O_i - \bar{O}|)^2} \quad \# \quad (15)$$

where n is the number of measurements, P_i is the simulated value, O_i is the observed value, \bar{O} is the observed mean value and \bar{P} is the average of simulated data. A good agreement between measured and simulated data is indicated by NRMSE values near to zero. On the other hand, when the EF values are near to 1, the model's performance is considered satisfactory.

3. Results

3.1. Sensitivity analysis

3.1.1. Morris method

The five most influential parameters for the canopy cover, biomass and yield responses (as identified by the main effect μ^*) are ranked in Table 5. Only those with μ^* greater than 0.1 were ranked. The number of

non-influential factors differs slightly from one field to another. Ten non-sensitive factors were identified for yield, 6 for aboveground biomass and 12 for canopy cover as shown in Table 6.

The yield sensitivity analysis revealed that the most sensitive parameters for most of the fields were the normalized water productivity (Wp) and the reference harvest index ($Hi0$). Parameters related to root development (Zx , Zn , $WxTopZ$, $WxBotZ$), crop phenology ($gYld$), crop transpiration (Kcb) and water stress ($pPolLo$, $pExpLo$) exhibited high interactions between each other. Aboveground biomass was most sensitive to water productivity (Wp) and other parameters related to crop transpiration and development (Kcb , CGC). The Morris results for the canopy cover indicated that the parameters related to root development ($WxTopZ$, $WxBotZ$) were most sensitive for wheat grown in the first season. The canopy cover was most sensitive to crop development and phenology parameters (CDC , $gSen$) in the second growing season (2003–2004).

3.1.2. FAST method

First order sensitivity indices were calculated for the remaining input parameters from the Morris step using FAST method. Fig. 3 illustrates the main effect sensitivity index time series for CC in days after sowing. The results show that $gEme$, $gMat$, CGC and $WxBotZ$ were the most sensitive parameters for the studied parcels. The canopy growth coefficient (CGC) and the time from sowing to emergence ($gEme$) were sensitive at the beginning of the season while the canopy decline coefficient (CDC), the time from sowing to maturity and senescence (i.e., $gMat$, $gSen$) were more influential at the end of the season. Finally, the most water stress sensitive parameters in mid-season were related to the stomatal control ($pStmLo$), while the canopy expansion and senescence water stress parameters (i.e., $pExpLo$, $pSenUp$) were more sensitive at the beginning of the season.

Aboveground biomass FAST analysis findings are displayed in Fig. 4.

Table 6

Non-influential parameters that are common for all studied fields according to the Morris Analysis. Min and Max represent the minimum and maximum Morris mean of elementary effects (μ^*) in the studied parcels.

Output Response	Non-Influential Parameters	Min	Max	
Yield	sPol	0.02	0.08	
	pPolLo	0.03	0.09	
	pPolUp	0.01	0.07	
	Aer	0.05	0.08	
	dxHi0	0.08	0.1	
	sZsp	0.02	0.06	
	sStm	0.04	0.09	
	gZx	0.03	0.07	
	Zn	0.01	0.05	
	exF	0.06	0.09	
	Aboveground Biomass	sPol	0.02	0.05
		pPolUp	0.04	0.08
pPolLo		0.01	0.06	
exF		0.03	0.07	
Aer		0.07	0.09	
dxHi0		0.05	0.08	
Canopy Cover	dxHi0	0.04	0.06	
	Wpy	0.03	0.09	
	Wp	0.02	0.08	
	Hi0	0.01	0.07	
	exF	0.06	0.09	
	sPol	0.02	0.08	
	cdAge	0.03	0.09	
	pPolUp	0.01	0.05	
	pPolLo	0.04	0.08	
	Aer	0.05	0.07	
	sStm	0.03	0.06	
	gYldDur	0.07	0.09	

The results showed that the crop phenological parameters (i.e., $gEme$, $gMat$, $gSen$), the canopy development parameters (i.e., CGC , CDC , CCX , Kcb) and the biomass production parameters (i.e., Wp , Wpy) were the common sensitive parameters for the investigated parcels. The time from sowing to emergence ($gEme$) was sensitive at the beginning of the season and its sensitivity decreased gradually over time. Meanwhile, the time from sowing to both senescence and maturity was only sensitive at the end of the season. The parameters related to the canopy expansion and the biomass production (i.e., CGC , Wp) were influential during the whole season period. While the canopy decline coefficient (CDC) and the maximum water extraction at top and bottom of the root zone ($WxTopZ$, $WxBotZ$) were mostly influential and the end and the mid-season respectively.

The SA results for yield (Fig. 5) showed that the most sensitive parameters were the normalized water productivity (Wp), the reference harvest index ($Hi0$), the maximum canopy cover coefficient (Kcb), the Adjustment of water productivity parameter in yield formation stage (Wpy), the canopy growth coefficient (CGC) and the Lower soil water depletion threshold for water stress effects on canopy expansion ($pExpLo$). Overall, the yield analysis showed that the reference harvest index ($Hi0$) and the normalized water productivity (Wp) were sensitive for all parcels.

3.2. Optimization

3.2.1. Canopy cover

For the calibration set (A1 – A3), simulated and measured CC that resulted from the two fits (one based on hemispherical photography, the other on remote sensing) were in good agreement (Table 7). When CC was simulated based on hemispherical photography predictions (PSO_{HP}), the estimated canopy cover CC_{HP} corresponded extremely well with the observed CC with R^2 values >0.98 , low estimation errors (6.39% NRMSE), high D-index (>0.99), and D-index (>0.98). The remote sensing-based optimization (PSO_{L7}) in the calibration set revealed a similar but less precise match between observed and simulated canopy cover values compared to PSO_{HP} with an R^2 , NRMSE, D-

index and EF of 0.72, 28.97%, 0.9 and 0.71 respectively.

The observed canopy cover from Landsat7 seems to be higher than that derived from hemispherical imagery at the beginning of the season as shown in Fig. 6. This induced PSO_{L7} to have an earlier crop emergence and a higher canopy growth coefficient values ($gEme= 47.25$, $CGC=0.011$) than PSO_{HP} ($gEme= 98.56$, $CGC= 0.01$) as indicated in Appendix B, Table B.1. In addition, a strong canopy decline coefficient ($CDC= 0.0049$) was identified in PSO_{HP} , resulted in a rapid drop of the canopy and lesser growing degree days to reach the maturity ($gMat = 1472.10$), while a lesser CDC ($CDC = 0.004$) was observed in PSO_{L7} , resulted in a delayed maturity of the crop ($gMat = 1500$). For complete model parametrization sets, see Table B.1 in Appendix B.

The validation set revealed that canopy cover predicted using hemispherical photographs led to better model parametrization compared to Landsat7. Overall, the observed and simulated canopy cover were in good agreement, as shown by low NRMSE, and high R^2 , D-index and EF values in Table 7.

3.2.2. Yield

Winter wheat yields measured in the field experiments ranged from 0.9 t/ha to 3.26 t/ha, while simulated values using hemispherical photographs and remote sensing parametrizations ranged from 1.14 t/ha and 1.29 t/ha to 3.9 t/ha and 3.8 t/ha, respectively as shown in Fig. 7. The R^2 between measured and simulated yield using PSO_{HP} and PSO_{L7} in the calibration dataset was equal to 0.89 and 0.99 (Table 8). Overall, the application of PSO with hemispherical and Landsat7 extracted canopy cover simulated the yield with low estimation errors and high efficiency in the calibration set. In the validation set, hemispherical photography-based parametrization produced better yield estimates ($R^2=0.44$, D-index= 0.75, EF=0.04) and lower estimation errors (NRMSE= 25.4%) compared to the other approach (i.e., PSO_{L7}). It is important to note that while simulating yield using PSO_{L7} , a negative EF was found, indicating that the mean of the observations gives a better prediction than the model.

4. Discussion

4.1. Insights from Morris and FAST sensitivity analysis of AquaCrop parameters

Many research studies have calibrated AquaCrop using field data (López-Urrea et al., 2020; Wellens et al., 2022). However, most of them have fine-tuned the parameters using trial and error. We present a practical method for parameterizing AquaCrop using a two-step optimization; first by selecting the set the influential parameters then fitting the canopy cover and then the yield.

To inform our optimisation, we used Morris and FAST sensitivity analyses to determine the most influential parameters of AquaCrop. Many studies have demonstrated that just a few parameters out of the model's large number have a substantial influence on the model's output (DeJonge et al., 2012; Sarrazin et al., 2016). DeJonge et al. (2012) performed both Morris and Sobol variance-based methods on CERES-Maize input parameters affecting the crop growth and found that while considering the anthesis day after planting (ADAY) output, only two out the model parameters were sensitive for both full and limited irrigation treatments. Our results agree with this observation. We discovered that only 24 out of 36 model parameters influenced the canopy cover significantly and only 26 for the yield. Moreover, our results showed that Morris and FAST do not always agree on the priority ranking of a parameter. As an example, Morris prioritized the time from sowing to start of yield formation ($gYld$) for yield prediction, but the lower soil water depletion threshold for water stress effects on stomatal control ($pStmLo$) was found to be the most influential parameter when using the FAST method for the parcel B6. This finding aligns with Confalonieri et al. (2010) who analysed different sensitivity analysis outcomes of the rice crop model WARM and concluded that in nonlinear

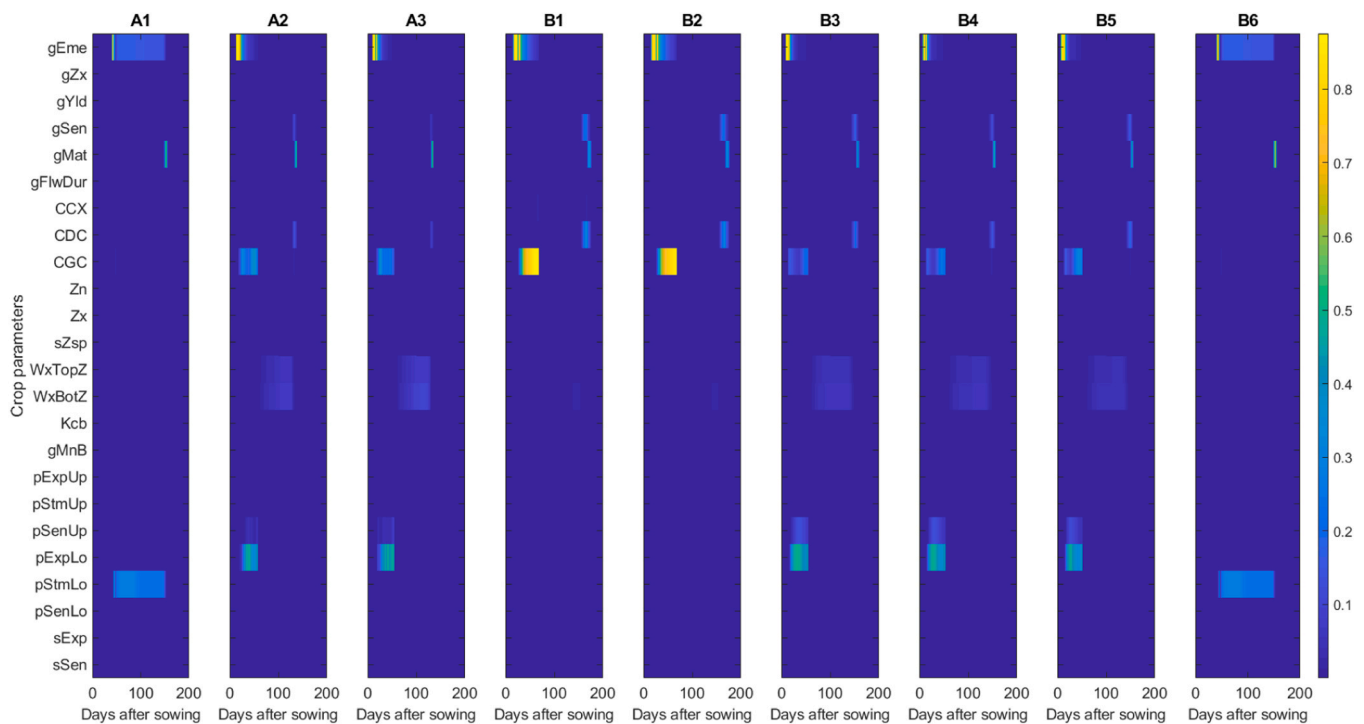


Fig. 3. FAST analysis results for the canopy cover time series. Parcels B1 and B2, sown earlier, exhibited lower water stress due to additional rainfall.

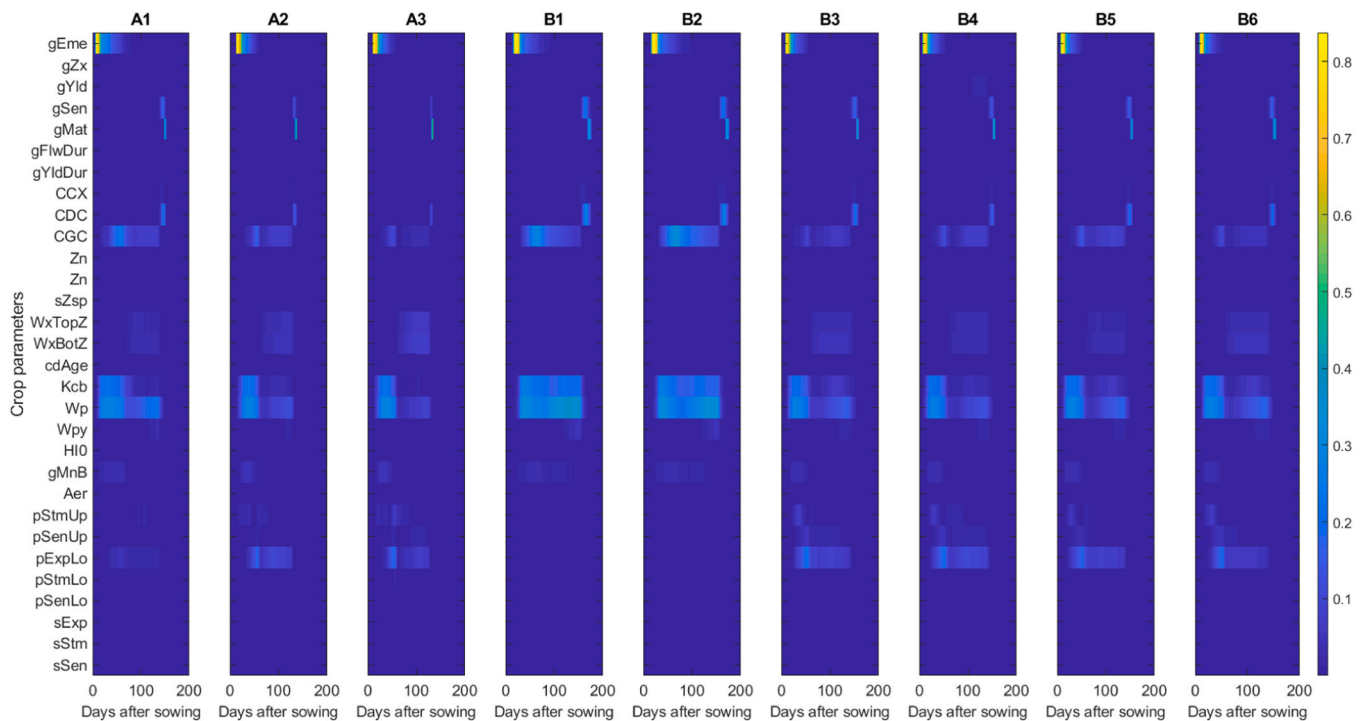


Fig. 4. FAST analysis results for the aboveground biomass time series. Parcels B1 and B2, sown earlier, exhibited lower water stress due to additional rainfall.

models or when the number of model trajectories is small, Morris versus variance-based approaches may order parameters differently. They concluded that the simplest approach (i.e., Morris) achieved equivalent outcomes to those reached by computationally intensive methods. We also found that the sensitive factors were generally consistent across the fields considered in our study. There were a few exceptions. Water stress factors (*pStmUp*, *pSenUp*, *pExpLo*) had no effect on simulating canopy cover in fields B1 and B2. These fields were sown early and so it is likely that they benefited from early rainfall mitigating effects of water stress. This has been reported in other studies including Xing et al. (2017) who

reported that *pSenUp* was more sensitive in plants under water stress. Therefore, although we can anticipate similar sets of parameters to be influential across seasons and locations, they will change significantly according to climate and local environmental factors.

4.2. Impact of the source of canopy cover on the predictive performance of AquaCrop

Investigating the impact of various sources of canopy measures on prediction accuracy and considering the practical implications of

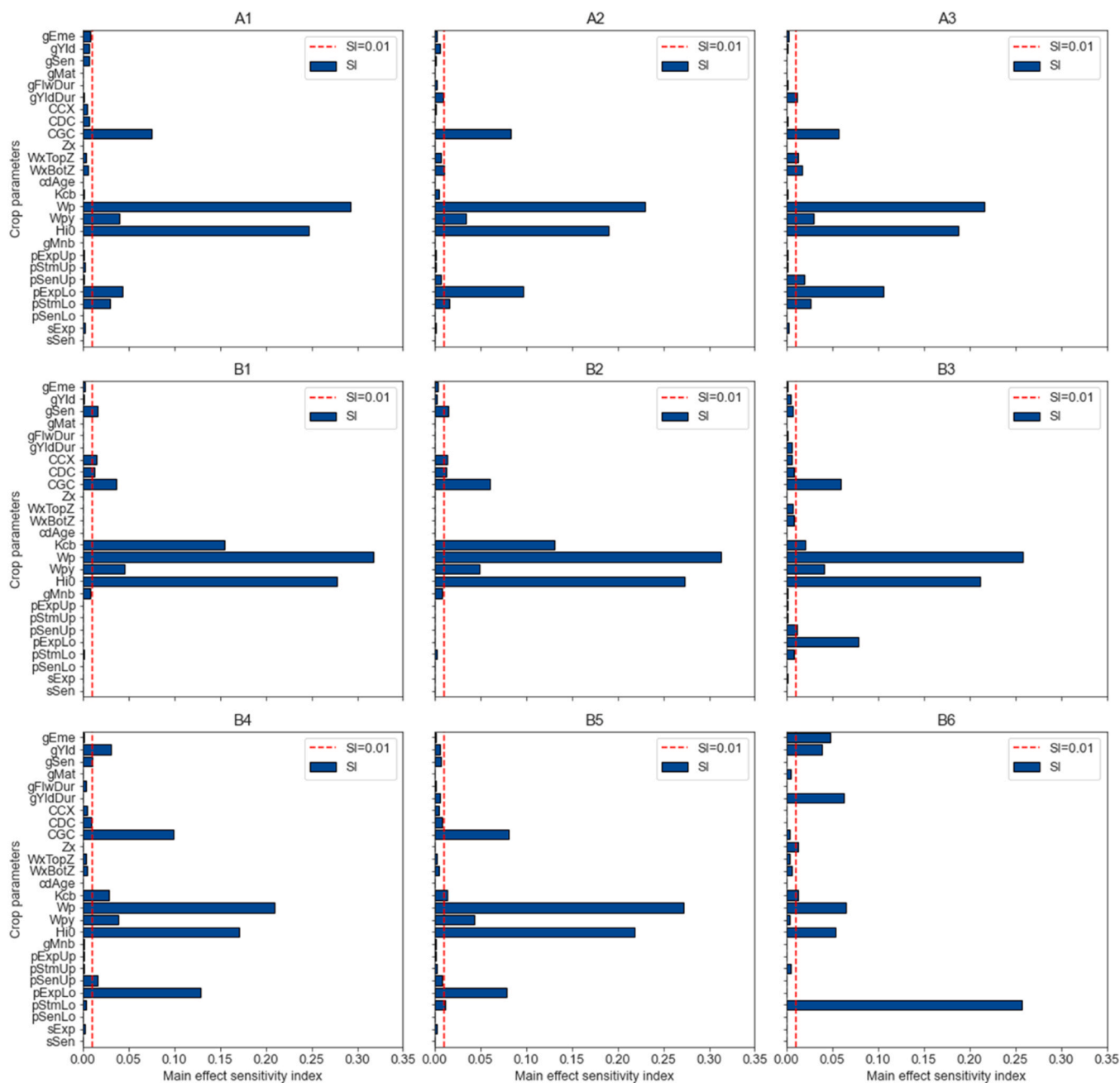


Fig. 5. FAST analysis results for the yield with cut-off value (horizontal red dashed line).

Table 7

Model performance indicators comparing observed and simulated canopy cover.

Performance indicator	Hemispherical photography		Landsat7	
	Calibration	Validation	Calibration	Validation
R ²	0.98	0.76	0.72	0.62
NRMSE (%)	6.39	45.87	28.97	51.37
D-index	0.99	0.90	0.90	0.86
EF	0.98	0.63	0.71	0.54

sourcing these measures are critical aspects in understanding the influence of different parametrization methods on AquaCrop’s predictions. Notably, good agreement was found between the simulated and observed canopy cover when using Landsat7 parametrization (PSO_{L7}), although it was less accurate when compared to the hemispherical photography-based parametrizations (PSO_{HP}). This could be explained

by the effect of soil brightness on NDVI at low vegetative cover, which leads to an overestimation of the canopy cover at the beginning of the growing season, hence predicting an accelerated crop emergence (47.25 GDDs when simulating with CC_{L7} against 98.56 GDDs when simulating with CC_{HP}). Another aspect in favour of hemispherical photography parametrization is the saturation effect of satellite-based products and particularly NDVI at high vegetative cover in our scenario. Consequently, the simulated canopy cover tended to be underestimated at high vegetation density at mid-season, resulting in a shorter time period for the crop to reach senescence compared to the other type of parametrization (gSen_{L7}=610.99, gSen_{HP}=817.6). Aboveground biomass offers an alternative state variable that can be used to optimise the parameterisation of the AquaCrop canopy; and it is more directly related to yield prediction than canopy cover (see Section 2.1). However similar to canopy cover, predictions of aboveground biomass made from optical vegetation indices are subject to spectral saturation issues. Combining

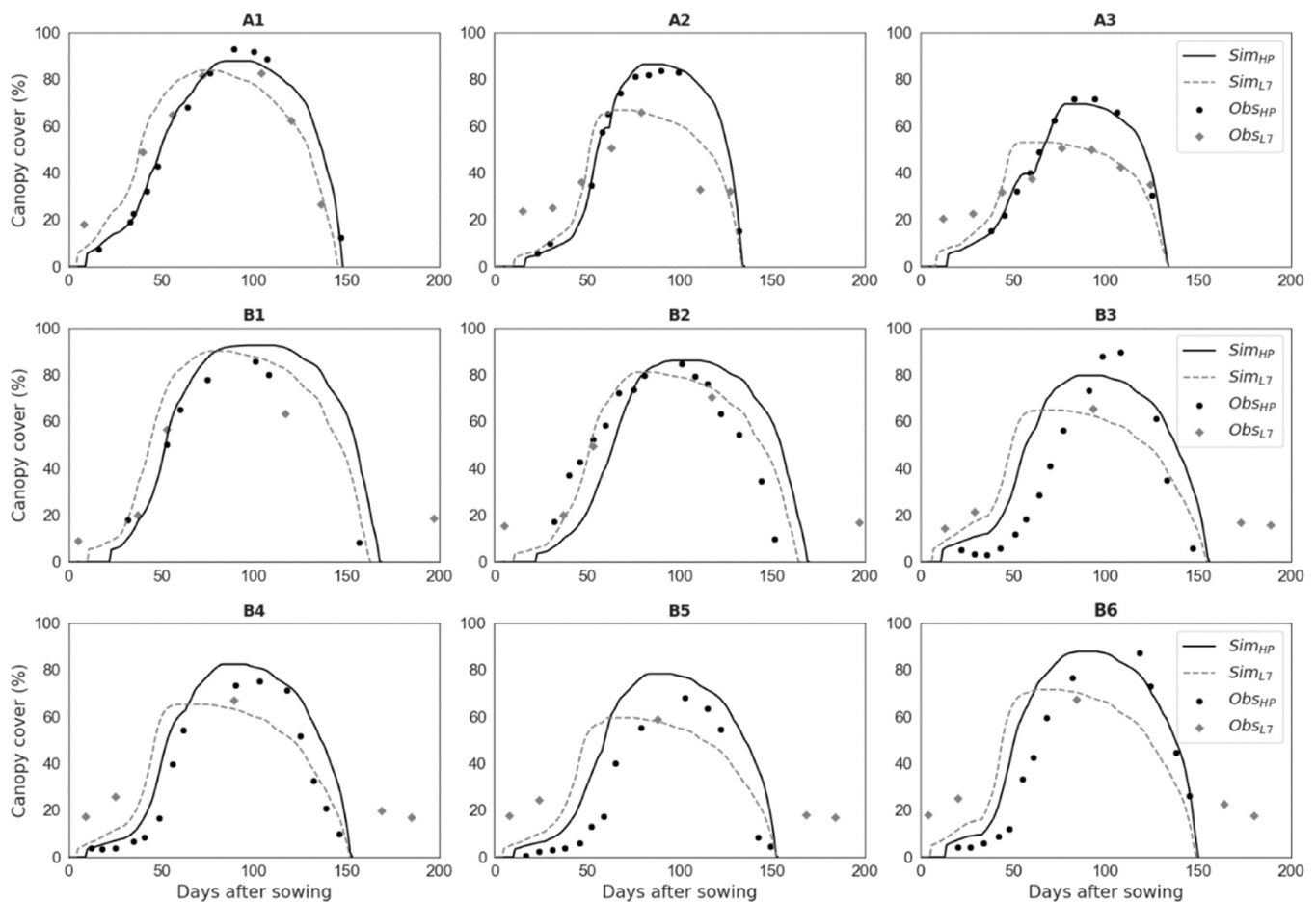


Fig. 6. Comparison of model simulated canopy cover using hemispherical photography, Landsat7 and field observed canopy cover using hemispherical photography and Landsat7. Where Sim_{HP} and Sim_{L7} represent the simulated canopy cover by AquaCrop using Hemispherical photography and Landsat7 parametrisation sets, respectively. While Obs_{HP} and Obs_{L7} denote the field observed canopy cover using hemispherical photographs and Landsat7 imagery, respectively.

measures of vegetation indices with Lidar or texture features has the potential to address these limitations (Yue et al., 2017). Liu et al. (2022a) used data from unmanned aerial vehicles and found combining estimates of texture and crop height greatly reduced problems associated with saturation. Similarly, Liu et al. (2023) and Liu et al. (2022b)

addressed the problem of spectral saturation in estimating potato aboveground biomass (AGB) through applying remote sensing techniques to acquire RGB and hyperspectral images of potato growth stages from a high-definition digital camera sensor. The findings demonstrated that the accuracy of predictions under high coverage was improved by

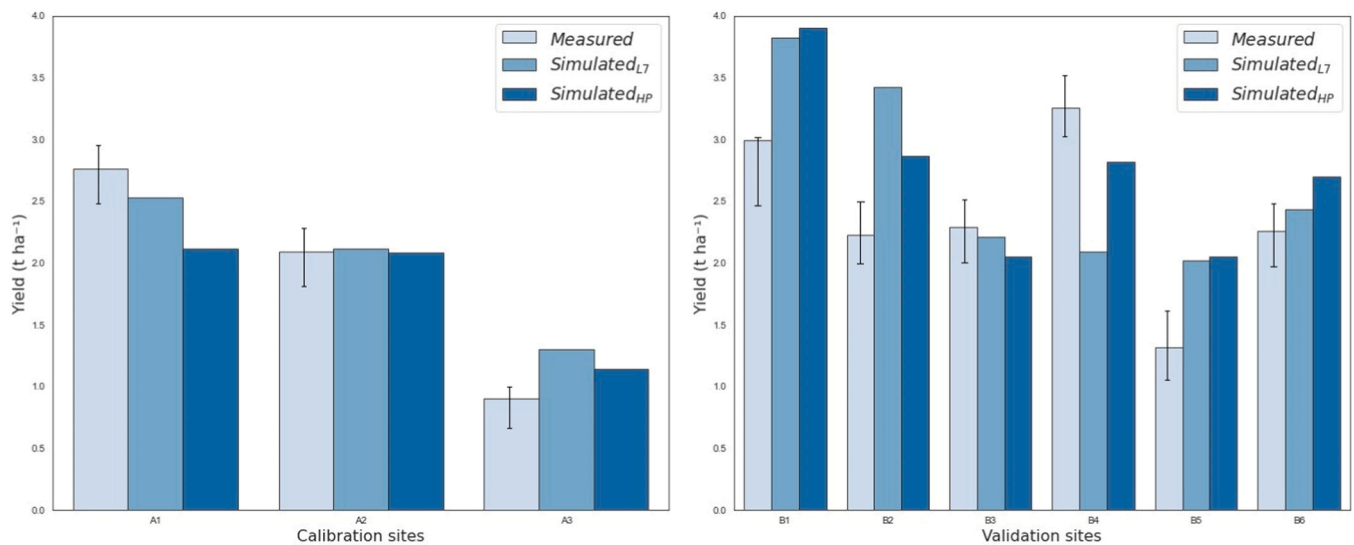


Fig. 7. Comparison of model simulated yield using hemispherical photography, Landsat7 and field observed yield in the calibration sites (left) and the validation sites (right). $Simulated_{L7}$ and $Simulated_{HP}$ denote the AquaCrop simulated yield using Landsat7 and hemispherical photography parameterisations, respectively. The whiskers represent the minimum and maximum of the observed yield values (See Table 3).

Table 8
Model performance indicators comparing observed and simulated yield.

Performance indicator	Hemispherical photography		Landsat7	
	Calibration	Validation	Calibration	Validation
R ²	0.89	0.44	0.99	0.10
NRMSE (%)	20.63	25.4	13.86	34.23
D-index	0.89	0.75	0.95	0.55
EF	0.73	0.04	0.88	-0.73

fusing optical features (including RGB and hyperspectral vegetation indices), structural features (i.e., canopy fluctuation rate, crop height and coverage) and textural features. These integrative approaches therefore show great promise where appropriate data are available.

Another key limitation with the Landsat 7 was the numbers of observations available across the season. At the time of the study passes occurred every 16 days. In the past five years there has been a rapid increase in the number of EO satellites, now medium resolution imagery (10–30 m pixels) is freely available every few days (Li and Chen, 2020). Other studies have explored the effect of the source of canopy cover measures on the accuracy of predictions. For example, Ma et al. (2017) considered the reliability of canopy cover retrieval from three different data types (LIDAR, aerial photography, and spaceborne imaging) and found that spaceborne WorldView2 (1.84 m pixel) data produced the highest accuracy ($R^2 = 0.58$), followed by aerial imagery ($R^2 = 0.50$) and LIDAR data ($R^2 = 0.33$). Jin et al. (2020) conducted a similar method of parameter optimization with PSO to determine the yield of maize in China using hyperspectral data from a spectrometer. They demonstrated that the enhanced vegetation index (EVI) could be used to estimate CC more accurately than other vegetation indices such as NDVI ($R^2 = 0.78$ and RMSE = 9.84%). In a separate study, Jin et al. (2017) compared the results of the assimilation of optical and radar imaging data in China using the PSO algorithm. They found that the estimated CC obtained from RADARSAT-2 data outperformed HJ-1A/B optical data, indicating that the source of canopy cover data is a crucial factor affecting the model parametrizations.

The empirical relationship between CC and NDVI is widely used (Gamon et al., 1995; Tsakmakis et al., 2021; Yang et al., 2017). However, its accuracy is subject to uncertainties related to factors, covering atmospheric conditions (Agapiou et al., 2011), sunlight angle (Ishihara et al., 2015), soil properties (Prudnikova et al., 2019), and vegetation types (Huemmerich et al., 2021; Zou and Möttus, 2017). Despite the goodness of fit of the NDVI-CC relationship ($R^2 = 0.71$), these uncertainties may in part explain the poor performance of the L7 parametrization as compared to the hemispherical-based parametrization.

The accuracy of AquaCrop's yield predictions is reported to be strongly linked with the quality of the canopy cover simulations (Hsiao et al., 2009). This is consistent with our findings; our parametrization based on hemispherical photography data produced superior yield prediction results (Table 8). The obvious improvements in prediction accuracy from using the hemispherical photography-based compared with using Landsat 7 come at a cost. Hemispherical photographs required human intervention in the field (in our case eleven times per season). For each field, many photographs were taken to get an estimate of the mean canopy cover. As a result, the time and effort required grows proportionally with the number of taken photographs. Finally, the ability to use hemispherical photography is partially limited by the weather, since measurements may be missed due to rain, wind, or inaccessibility to the research site. Thus, coupling canopy cover observations extracted from both satellite imagery and hemispherical photographs is highly recommended to alleviate some of the weather-related constraints and subsequently improve yield simulations.

5. Conclusions

In this study, we carried out a two-stage sensitivity analysis (Morris and FAST) of crop canopy cover and yield for the FAO-AquaCrop model, in which we incorporated algorithms to account for the impact of soil fertility on canopy cover growth, maximum canopy cover, and biomass water productivity. The sensitivity analysis results revealed that canopy cover predictions were most sensitive to parameters related to emergence and maturity timing as well as the canopy growth rate. For our study area, the influential parameters were generally consistent across seasons and fields with the exception of those related to water stress. This shows the importance of selecting sensitive parameters for a site based on data from several seasons or variation in sowing time. Our findings showed that the hemispherical photography-based parameterization outperformed the satellite-based parameterization for canopy cover and yield simulations using AquaCrop. Although simulations of the Landsat 7 observed canopy were reasonable in the validation set, they were not as accurate as those from hemispherical photographs and the associated yield predictions were particularly poor. This highlights the importance of accurate canopy cover predictions in estimating final yield. Overall, our research demonstrates the usefulness and efficiency of the proposed optimization procedure in capturing the full range of model parameters using different source of data while accommodating the unique characteristics of the study area. Further research may be needed to examine the potential improvements in prediction that could be achieved by integrating different types of canopy cover data (Hybrid models, portable instruments, UAV, Radar, and optical data) or by updating the model predictions in real-time as new observations become available.

Funding

This project is funded by Office Chérifien des Phosphates (OCP group) through the collaboration between Cranfield University (CU), Rothamsted Research (RRes) and Mohammed VI Polytechnic University (UM6P).

CRedit authorship contribution statement

Bader Oulaid: Writing – review & editing, Writing – original draft, Visualization, Validation, Software, Resources, Project administration, Methodology, Investigation, Formal analysis, Data curation, Conceptualization. **Alice E. Milne:** Writing – review & editing, Writing – original draft, Visualization, Validation, Supervision, Software, Resources, Project administration, Methodology, Investigation, Funding acquisition, Formal analysis, Data curation, Conceptualization. **Toby Waime:** Writing – review & editing, Writing – original draft, Visualization, Validation, Supervision, Project administration, Methodology, Investigation, Conceptualization. **Rafiq El Alami:** Writing – review & editing, Writing – original draft, Visualization, Validation, Supervision, Software, Resources, Project administration, Methodology, Investigation, Funding acquisition, Formal analysis, Data curation, Conceptualization. **Maryam Rafiqi:** Resources, Project administration, Methodology, Conceptualization. **Ron Corstanje:** Writing – review & editing, Writing – original draft, Visualization, Validation, Supervision, Software, Resources, Project administration, Methodology, Investigation, Funding acquisition, Formal analysis, Data curation, Conceptualization.

Declaration of Competing Interest

The authors declare that they have no known competing financial interests or personal relationships that could have appeared to influence the work reported in this paper.

Data Availability

Data supporting this study are included within the article and/or supporting materials

Acknowledgments

This work is part of the SAFA (Sustainable Agriculture For Africa) project which is funded by OCP, Morocco.

Appendix A. Daily meteorological data

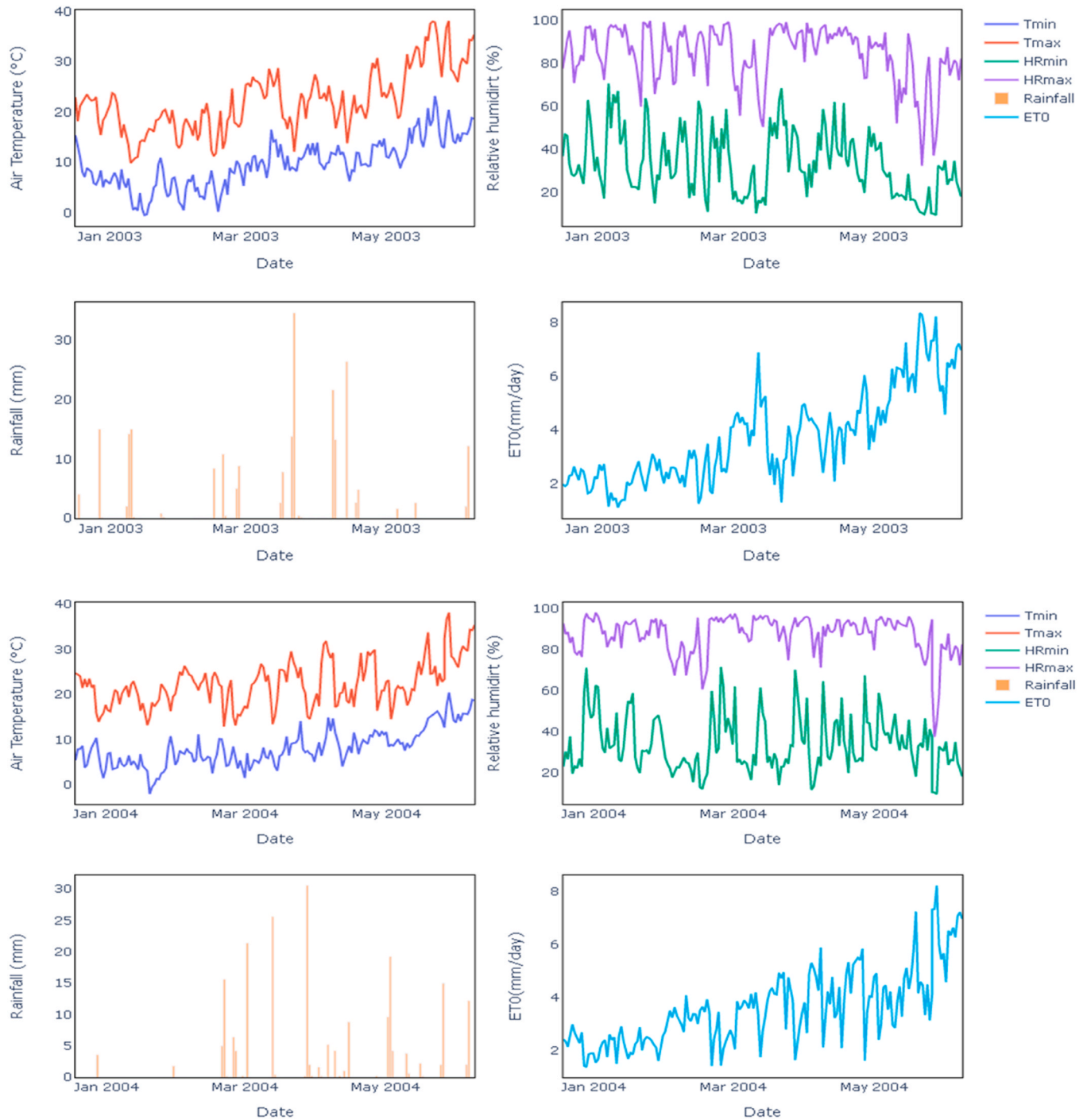


Fig. A1. Daily meteorological data on the experimental site for the 2002–2003 and 2002–2003 growing seasons.

Appendix B. AquaCrop model main parameter list

Table B.1

AquaCrop main sensitive model parameters values obtained using the two studied approaches

Input Parameters	Parametrization	
	PSO _{L7}	PSO _{HP}
gEme	47.250	98.56
gMat	1500	1472.10
gSen	610.99	817.63
CDC	0.004008	0.004929
CGC	0.011127	0.010551
CCX	0.97	0.95
WxTopZ	0.014176	0.05881
WxBotZ	0.002124	0.058738
pExpLo	0.719999	0.719994
pStmLo	0.741239	0.699532
pStmUp	0.354651	0.34125
pSenUp	0.946777	0.858135
sExp	4.874926	4.87476
gYld	455.72	641.55
gYldDur	748.94	669
Kcb	1.785033	0.579192
Wp	27.5	20
Wpy	56.25	156.25
Hi0	0.31596	0.249975

References

- Abi Saab, M.T., el Alam, R., Jomaa, I., Skaf, S., Fahed, S., Albrizio, R., Todorovic, M., 2021. Coupling remote sensing data and aquacrop model for simulation of winter wheat growth under rainfed and irrigated conditions in a mediterranean environment. *Agronomy* 11. <https://doi.org/10.3390/agronomy11112265>.
- Agapiou, A., Hadjimitsis, D.G., Papoutsas, C., Alexakis, D.D., Papadavid, G., 2011. The Importance of accounting for atmospheric effects in the application of NDVI and interpretation of satellite imagery supporting archaeological research: The case studies of Palaepaphos and Nea Paphos sites in Cyprus. *Remote Sens (Basel)* 3, 2605–2629. <https://doi.org/10.3390/rs3122605>.
- Akbari, R., Mohammadi, A., Ziarati, K., 2010. A novel bee swarm optimization algorithm for numerical function optimization. *Commun. Nonlinear Sci. Numer. Simul.* 15, 3142–3155. <https://doi.org/10.1016/j.cnsns.2009.11.003>.
- Benabdelouahab, T., Balaghi, R., Hadria, R., Lionboui, H., Djaby, B., Tychon, B., 2016. Testing aquacrop to simulate durum wheat yield and schedule irrigation in a semi-arid irrigated perimeter in Morocco. *Irrig. Drain.* 65, 631–643. <https://doi.org/10.1002/ird.1977>.
- Campolongo, F., Cariboni, J., Saltelli, A., 2007. An effective screening design for sensitivity analysis of large models. *Environ. Model. Softw.* 22, 1509–1518. <https://doi.org/10.1016/j.envsoft.2006.10.004>.
- Casa, R., Varella, H., Buis, S., Guérif, M., De Solan, B., Baret, F., 2012. Forcing a wheat crop model with LAI data to access agronomic variables: evaluation of the impact of model and LAI uncertainties and comparison with an empirical approach. *Eur. J. Agron.* 37, 1–10. <https://doi.org/10.1016/j.eja.2011.09.004>.
- Choruma, D.J., Balkovic, J., Pietsch, S.A., Odume, O.N., 2021. Using EPIC to simulate the effects of different irrigation and fertilizer levels on maize yield in the Eastern Cape, South Africa. *Agric. Water Manag.* 254. <https://doi.org/10.1016/j.agwat.2021.106974>.
- Ciric, C., Ciffroy, P., Charles, S., 2012. Use of sensitivity analysis to identify influential and non-influential parameters within an aquatic ecosystem model. *Ecol. Model.* 246, 119–130. <https://doi.org/10.1016/j.ecolmodel.2012.06.024>.
- Confalonieri, R., Bellocchi, G., Bregaglio, S., Donatelli, M., Acutis, M., 2010. Comparison of sensitivity analysis techniques: a case study with the rice model WARM. *Ecol. Model.* 221, 1897–1906. <https://doi.org/10.1016/j.ecolmodel.2010.04.021>.
- Cukier, R.I., Fortuin, C.M., Shuler, K.E., Petschek, A.G., Schaibly, J.H., 1973. Study of the sensitivity of coupled reaction systems to uncertainties in rate coefficients. I Theory. *J. Chem. Phys.* 59, 3873–3878. <https://doi.org/10.1063/1.1680571>.
- DeJonge, K.C., Ascough, J.C., Ahmadi, M., Andales, A.A., Arabi, M., 2012. Global sensitivity and uncertainty analysis of a dynamic agroecosystem model under different irrigation treatments. *Ecol. Model.* 231, 113–125. <https://doi.org/10.1016/j.ecolmodel.2012.01.024>.
- Dhillon, M.S., Dahms, T., Kuebert-Flock, C., Borg, E., Conrad, C., Ullmann, T., 2020. Modelling crop biomass from synthetic remote sensing time series: Example for the DEMMIN test site, Germany. *Remote Sens (Basel)* 12. <https://doi.org/10.3390/rs12111819>.
- Dirwai, T.L., Senzanje, A., Mabhaudhi, T., 2021. Calibration and evaluation of the fao aquacrop model for canola (*Brassica napus*) under varied moisture irrigation regimes. *Agriculture* 11. <https://doi.org/10.3390/agriculture11050410>.
- Dong, Y., Zhao, C., Yang, G., Chen, L., Wang, J., Feng, H., 2013. Integrating a very fast simulated annealing optimization algorithm for crop leaf area index variational assimilation. *Math. Comput. Model.* 58, 877–885. <https://doi.org/10.1016/j.mcm.2012.12.013>.
- Doorenbos, J., Kassam, A.H., Bentvelsen, C.I.M., 1979. Yield response to water. Food and Agriculture Organization of the United Nations.
- Er-Raki, S., Bouras, E., Rodriguez, J.C., Watts, C.J., Lizarraga-Celaya, C., Chehbouni, A., 2021. Parameterization of the AquaCrop model for simulating table grapes growth and water productivity in an arid region of Mexico. *Agric. Water Manag.* 245. <https://doi.org/10.1016/j.agwat.2020.106585>.
- Foster, T., Brozović, N., Butler, A.P., Neale, C.M.U., Raes, D., Steduto, P., Fereres, E., Hsiao, T.C., 2017. AquaCrop-OS: an open source version of FAO's crop water productivity model. *Agric. Water Manag.* 181, 18–22. <https://doi.org/10.1016/j.agwat.2016.11.015>.
- Gamon, J.A., Field, C.B., Goulden, M.L., Griffin, K.L., Hartley, A.E., Joel, G., Penuelas, J., Valentini, R., 1995. Relationships between NDVI, canopy structure, and photosynthesis in three Californian vegetation types. *Ecol. Appl.* 5, 28–41. <https://doi.org/10.2307/1942049>.
- Gorelick, N., Hancher, M., Dixon, M., Ilyushchenko, S., Thau, D., Moore, R., 2017. Google Earth Engine: planetary-scale geospatial analysis for everyone. *Remote Sens Environ.* 202, 18–27. <https://doi.org/10.1016/j.rse.2017.06.031>.
- Greaves, G.E., Wang, Y.M., 2016. Assessment of fao aquacrop model for simulating maize growth and productivity under deficit irrigation in a tropical environment. *Water (Switz.)* 8. <https://doi.org/10.3390/w8120557>.
- Hariharan, G., Kannan, K., 2014. Review of wavelet methods for the solution of reaction-diffusion problems in science and engineering. *Appl. Math. Model.* 38, 799–813. <https://doi.org/10.1016/j.apm.2013.08.003>.
- Hsiao, T.C., Heng, L., Steduto, P., Rojas-Lara, B., Raes, D., Fereres, E., 2009. Aquacrop-The FAO crop model to simulate yield response to water: III. parameterization and testing for maize. *Agron. J.* 101, 448–459. <https://doi.org/10.2134/agronj2008.0218s>.
- Huemmerich, K.F., Vargas Zesati, S., Campbell, P., Tweedie, C., 2021. Canopy reflectance models illustrate varying NDVI responses to change in high latitude ecosystems. *Ecol. Appl.* 31. <https://doi.org/10.1002/eap.2435>.
- Iqbal, M.A., Shen, Y., Stricevic, R., Pei, H., Sun, H., Amiri, E., Penas, A., del Rio, S., 2014. Evaluation of the FAO AquaCrop model for winter wheat on the North China Plain under deficit irrigation from field experiment to regional yield simulation. *Agric. Water Manag.* 135, 61–72. <https://doi.org/10.1016/j.agwat.2013.12.012>.
- Ishihara, M., Inoue, Y., Ono, K., Shimizu, M., Matsuura, S., 2015. The impact of sunlight conditions on the consistency of vegetation indices in croplands-effective usage of vegetation indices from continuous ground-based spectral measurements. *Remote Sens* 7, 14079–14098. <https://doi.org/10.3390/rs71014079>.
- Jin, X., Kumar, L., Li, Z., Xu, X., Yang, G., Wang, J., 2016. Estimation of winter wheat biomass and yield by combining the aquacrop model and field hyperspectral data. *Remote Sens* 8. <https://doi.org/10.3390/rs8120972>.
- Jin, X., Li, Z., Yang, G., Yang, H., Feng, H., Xu, X., Wang, J., Li, X., Luo, J., 2017. Winter wheat yield estimation based on multi-source medium resolution optical and radar imaging data and the AquaCrop model using the particle swarm optimization algorithm. *ISPRS J. Photogramm. Remote Sens.* 126, 24–37. <https://doi.org/10.1016/j.isprsjprs.2017.02.001>.
- Jin, X., Kumar, L., Li, Z., Feng, H., Xu, X., Yang, G., Wang, J., 2018. A review of data assimilation of remote sensing and crop models. *Eur. J. Agron.* <https://doi.org/10.1016/j.eja.2017.11.002>.

- Jin, X., Li, Z., Feng, H., Ren, Z., Li, S., 2020. Estimation of maize yield by assimilating biomass and canopy cover derived from hyperspectral data into the AquaCrop model. *Agric. Water Manag* 227. <https://doi.org/10.1016/j.agwat.2019.105846>.
- Jing, Q., McConkey, B., Qian, B., Smith, W., Grant, B., Shang, J., Liu, J., Bindraban, P., Luce, M.S., 2021. Assessing water management effects on spring wheat yield in the Canadian Prairies using DSSAT wheat models. *Agric. Water Manag* 244. <https://doi.org/10.1016/j.agwat.2020.106591>.
- Kennedy, J., Eberhart, R., 1995. Particle swarm optimization, in: *Proceedings of ICNN'95 - International Conference on Neural Networks*. IEEE, pp. 1942–1948. <https://doi.org/10.1109/ICNN.1995.488968>.
- Khabba, S., Duchemin, B., Hadria, R., Er-Raki, S., Ezzahar, J., Chehbouni, A., Lahrouni, A., Hanich, L., 2009. Evaluation of digital hemispherical photography and plant canopy analyzer for measuring vegetation area index of orange orchards. *J. Agron.* 8, 67–72. <https://doi.org/10.3923/ja.2009.67.72>.
- Khabba, S., Er-Raki, S., Toumi, J., Ezzahar, J., Hssaine, B.A., Page, M., Le, Chehbouni, A., 2020. A simple light-use-efficiency model to estimate wheat yield in the semi-Arid areas. *Agronomy* 10. <https://doi.org/10.3390/agronomy10101524>.
- Krishnan, M., Gugercin, S., Tarazaga, P.A., 2023. A wavelet-based dynamic mode decomposition for modeling mechanical systems from partial observations. *Mech. Syst. Signal Process* 187, 109919. <https://doi.org/10.1016/j.ymssp.2022.109919>.
- Li, J., Chen, B., 2020. Global revisit interval analysis of landsat-8-9 and sentinel-2a-2b data for terrestrial monitoring. *Sensors* 20, 1–15. <https://doi.org/10.3390/s20226631>.
- Li, Zhenhai, He, J., Xu, X., Jin, X., Huang, W., Clark, B., Yang, G., Li, Zhenhong, 2018. Estimating genetic parameters of DSSAT-CERES model with the GLUE method for winter wheat (*Triticum aestivum* L.) production. *Comput. Electron Agric.* 154, 213–221. <https://doi.org/10.1016/j.compag.2018.09.009>.
- Liu, Y., Feng, H., Yue, J., Jin, X., Li, Z., Yang, G., 2022a. Estimation of potato above-ground biomass based on unmanned aerial vehicle red-green-blue images with different texture features and crop height. *Front Plant Sci.* 13 <https://doi.org/10.3389/fpls.2022.938216>.
- Liu, Y., Feng, H., Yue, J., Li, Z., Yang, G., Song, X., Yang, X., Zhao, Y., 2022b. Remote-sensing estimation of potato above-ground biomass based on spectral and spatial features extracted from high-definition digital camera images. *Comput. Electron Agric.* 198 <https://doi.org/10.1016/j.compag.2022.107089>.
- Liu, Y., Feng, H., Yue, J., Fan, Y., Bian, M., Ma, Y., Jin, X., Song, X., Yang, G., 2023. Estimating potato above-ground biomass by using integrated unmanned aerial system-based optical, structural, and textural canopy measurements. *Comput. Electron Agric.* 213 <https://doi.org/10.1016/j.compag.2023.108229>.
- López-Urrea, R., Domínguez, A., Pardo, J.J., Montoya, F., García-Vila, M., Martínez-Romero, A., 2020. Parameterization and comparison of the AquaCrop and MOPECO models for a high-yielding barley cultivar under different irrigation levels. *Agric. Water Manag* 230. <https://doi.org/10.1016/j.agwat.2019.105931>.
- Lu, Y., Chibarabada, T.P., Ziliani, M.G., Onema, J.M.K., McCabe, M.F., Sheffield, J., 2021. Assimilation of soil moisture and canopy cover data improves maize simulation using an under-calibrated crop model. *Agric. Water Manag* 252. <https://doi.org/10.1016/j.agwat.2021.106884>.
- Lyu, J., Jiang, Y., Xu, C., Liu, Y., Su, Z., Liu, J., He, J., 2022. Multi-objective winter wheat irrigation strategies optimization based on coupling AquaCrop-OSPy and NSGA-III: a case study in Yangling, China. *Sci. Total Environ.* 843 <https://doi.org/10.1016/j.scitotenv.2022.157104>.
- Ma, Q., Su, Y., Guo, Q., 2017. Comparison of canopy cover estimations from airborne LiDAR, aerial imagery, and satellite imagery. *IEEE J. Sel. Top. Appl. Earth Obs. Remote Sens* 10, 4225–4236. <https://doi.org/10.1109/JSTARS.2017.2711482>.
- McRae, G.J., Tilden, J.W., Seinfeld, J.H., 1982. Global sensitivity analysis—a computational implementation of the fourier amplitude sensitivity test (FAST). *Comput. Chem. Eng.* 6, 15–25. [https://doi.org/10.1016/0098-1354\(82\)80003-3](https://doi.org/10.1016/0098-1354(82)80003-3).
- Morel, J., Bégué, A., Todoroff, P., Martiné, J.F., Lebourgeois, V., Petit, M., 2014. Coupling a sugarcane crop model with the remotely sensed time series of fPAR to optimise the yield estimation. *Eur. J. Agron.* 61, 60–68. <https://doi.org/10.1016/j.eja.2014.08.004>.
- Morris, M.D., 1991a. Factorial sampling plans for preliminary computational experiments. *Technometrics* 33, 161–174. <https://doi.org/10.1080/00401706.1991.10484804>.
- Morris, M.D., 1991b. Factorial Sampling Plans for Preliminary Computational Experiments, *TECHNOMETRICS*.
- Nash, J.E., Sutcliffe, J.V., 1970. River flow forecasting through conceptual models part I — a discussion of principles. *J. Hydrol. (Amst.)* 10, 282–290. [https://doi.org/10.1016/0022-1694\(70\)90255-6](https://doi.org/10.1016/0022-1694(70)90255-6).
- Ngwira, A.R., Aune, J.B., Thierfelder, C., 2014. DSSAT modelling of conservation agriculture maize response to climate change in Malawi. *Soil Tillage Res* 143, 85–94. <https://doi.org/10.1016/j.still.2014.05.003>.
- Nossent, J., Elsen, P., Bauwens, W., 2011. Sobol' sensitivity analysis of a complex environmental model. *Environ. Model. Softw.* 26, 1515–1525. <https://doi.org/10.1016/j.envsoft.2011.08.010>.
- Paleari, L., Movedi, E., Zoli, M., Burato, A., Cecconi, I., Errahouly, J., Pecollo, E., Sorvillo, C., Confalonieri, R., 2021. Sensitivity analysis using Morris: Just screening or an effective ranking method? *Ecol. Model.* 455, 109648 <https://doi.org/10.1016/j.ecolmodel.2021.109648>.
- Paredes, P., Wei, Z., Liu, Y., Xu, D., Xin, Y., Zhang, B., Pereira, L.S., 2015. Performance assessment of the FAO aquacrop model for soil water, soil evaporation, biomass and yield of soybeans in north china plain. *Agric. Water Manag* 152, 57–71. <https://doi.org/10.1016/j.agwat.2014.12.007>.
- Pelosi, A., Belfiore, O.R., D'Urso, G., Chirico, G.B., 2022. Assessing crop water requirement and yield by combining ERA5-land reanalysis data with CM-SAF satellite-based radiation data and sentinel-2 satellite imagery. *Remote Sens (Basel)* 14. <https://doi.org/10.3390/rs14246233>.
- Poempool, L., Kruatrachue, B., Siriboon, K., 2018. Combine multi particle swarm in supporting trapping in local optima, in: *ICEAST 2018 - 4th International Conference on Engineering, Applied Sciences and Technology: Exploring Innovative Solutions for Smart Society*. Institute of Electrical and Electronics Engineers Inc. <https://doi.org/10.1109/ICEAST.2018.8434398>.
- Prudnikova, E., Savin, I., Vindeker, G., Grubina, P., Shishkonakova, E., Sharychev, D., 2019. Influence of soil background on spectral reflectance of winter wheat crop canopy. *Remote Sens (Basel)* 11. <https://doi.org/10.3390/rs11161932>.
- Raes, D., Steduto, P., Hsiao, T.C., Fereres, E., 2009. Aquacrop-The FAO crop model to simulate yield response to water: II. main algorithms and software description. *Agron. J.* 101, 438–447. <https://doi.org/10.2134/agronj2008.0140s>.
- Ranghetti, L., Boschetti, M., Nutini, F., Busetto, L., 2020. sen2r™: An R toolbox for automatically downloading and preprocessing Sentinel-2 satellite data. *Comput. Geosci.* 139, 104473 <https://doi.org/10.1016/j.cageo.2020.104473>.
- Razzaghi, F., Zhou, Z., Andersen, M.N., Plauborg, F., 2017. Simulation of potato yield in temperate condition by the AquaCrop model. *Agric. Water Manag* 191, 113–123. <https://doi.org/10.1016/j.agwat.2017.06.008>.
- Sabzadeh, I., Shourian, M., 2020. Maximizing crops yield net benefit in a groundwater-irrigated plain constrained to aquifer stable depletion using a coupled PSO-SWAT-MODFLOW hydro-agronomic model. *J. Clean. Prod.* 262 <https://doi.org/10.1016/j.jclepro.2020.121349>.
- Sallati, A., Tarantola, S., Chan, K.P.-S., 1999. A quantitative model-independent method for global sensitivity analysis of model output. *Technometrics* 41, 39–56. <https://doi.org/10.1080/00401706.1999.10485594>.
- Sarrazin, F., Pianosi, F., Wagener, T., 2016. Global sensitivity analysis of environmental models: convergence and validation. *Environ. Model. Softw.* 79, 135–152. <https://doi.org/10.1016/j.envsoft.2016.02.005>.
- Schmidt, G., Jenkerson, C.B., Masek, J., Vermote, E., Gao, F., Survey, U.S.G., 2013. Landsat ecosystem disturbance adaptive processing system (LEDAPS) algorithm description, Open-File Report. Reston, VA. <https://doi.org/10.3133/ofr20131057>.
- Silvestro, P.C., Pignatti, S., Yang, H., Yang, G., Pascucci, S., Castaldi, F., Casa, R., 2017. Sensitivity analysis of the Aquacrop and SAFYE crop models for the assessment of water limited winter wheat yield in regional scale applications. *PLoS One* 12. <https://doi.org/10.1371/journal.pone.0187485>.
- Soltani, A., Alimaghani, S.M., Nehbandani, A., Torabi, B., Zeinali, E., Dadrasi, A., Zand, E., Ghassemi, S., Pourshirazi, S., Alasti, O., Hosseini, R.S., Zahed, M., Arabameri, R., Mohammadzadeh, Z., Rahban, S., Kamari, H., Fayazi, H., Mohammadi, S., Keramat, S., Vadez, V., van Ittersum, M.K., Sinclair, T.R., 2020. SSM-iCrop2: A simple model for diverse crop species over large areas. *Agric. Syst.* 182 <https://doi.org/10.1016/j.agsy.2020.102855>.
- Specka, X., Nendel, C., Wieland, R., 2015. Analysing the parameter sensitivity of the agro-ecosystem model MONICA for different crops. *Eur. J. Agron.* 71, 73–87. <https://doi.org/10.1016/j.eja.2015.08.004>.
- Steduto, P., Hsiao, T.C., Raes, D., Fereres, E., 2009. Aquacrop-the FAO crop model to simulate yield response to water: I. concepts and underlying principles. *Agron. J.* 101, 426–437. <https://doi.org/10.2134/agronj2008.0139s>.
- Stricevic, R., Cosic, M., Djurovic, N., Pejic, B., Maksimovic, L., 2011. Assessment of the FAO AquaCrop model in the simulation of rainfed and supplementally irrigated maize, sugar beet and sunflower. *Agric. Water Manag* 98, 1615–1621. <https://doi.org/10.1016/j.agwat.2011.05.011>.
- Szu, H., Hartley, R., 1987. Fast simulated annealing. *Phys. Lett. A* 122. [https://doi.org/10.1016/0375-9601\(87\)90796-1](https://doi.org/10.1016/0375-9601(87)90796-1).
- Takács, S., Csengeri, E., Pék, Z., Bíró, T., Szuvandzsev, P., Palotás, G., Helyes, L., 2021. Performance evaluation of aquacrop model in processing tomato biomass, fruit yield and water stress indicator modelling. *Water (Switz.)* 13. <https://doi.org/10.3390/w13243587>.
- Tenreiro, T.R., García-Vila, M., Gómez, J.A., Jiménez-Berni, J.A., Fereres, E., 2021. Using NDVI for the assessment of canopy cover in agricultural crops within modelling research. *Comput. Electron Agric.* 182 <https://doi.org/10.1016/j.compag.2021.106038>.
- Toumi, J., Er-Raki, S., Ezzahar, J., Khabba, S., Jarlan, L., Chehbouni, A., 2016a. Performance assessment of AquaCrop model for estimating evapotranspiration, soil water content and grain yield of winter wheat in Tensift Al Haouz (Morocco): application to irrigation management. *Agric. Water Manag* 163, 219–235. <https://doi.org/10.1016/j.agwat.2015.09.007>.
- Toumi, J., Er-Raki, S., Ezzahar, J., Khabba, S., Jarlan, L., Chehbouni, A., 2016b. Performance assessment of AquaCrop model for estimating evapotranspiration, soil water content and grain yield of winter wheat in Tensift Al Haouz (Morocco): application to irrigation management. *Agric. Water Manag* 163, 219–235. <https://doi.org/10.1016/j.agwat.2015.09.007>.
- Tsakmakis, I.D., Zoidou, M., Gikas, G.D., Sylaios, G.K., 2018. Impact of irrigation technologies and strategies on cotton water footprint using AquaCrop and CROPWAT models. *Environ. Process.* 5, 181–199. <https://doi.org/10.1007/s40710-018-0289-4>.
- Tsakmakis, I.D., Gikas, G.D., Sylaios, G.K., 2021. Integration of Sentinel-derived NDVI to reduce uncertainties in the operational field monitoring of maize. *Agric. Water Manag* 255, 106998. <https://doi.org/10.1016/j.agwat.2021.106998>.
- Upreti, D., Pignatti, S., Pascucci, S., Tolomio, M., Huang, W., Casa, R., 2020. Bayesian calibration of the Aquacrop-OS model for durum wheat by assimilation of canopy cover retrieved from VENUS satellite data. *Remote Sens (Basel)* 12. <https://doi.org/10.3390/rs12162666>.
- Vannoppen, A., Gobin, A., 2021. Estimating farm wheat yields from NDVI and meteorological data. *Agronomy* 11. <https://doi.org/10.3390/agronomy11050946>.

- Vanuytrecht, E., Raes, D., Willems, P., 2014. Global sensitivity analysis of yield output from the water productivity model. *Environ. Model. Softw.* 51, 323–332. <https://doi.org/10.1016/j.envsoft.2013.10.017>.
- Vazquez-Cruz, M.A., Guzman-Cruz, R., Lopez-Cruz, I.L., Cornejo-Perez, O., Torres-Pacheco, I., Guevara-Gonzalez, R.G., 2014. Global sensitivity analysis by means of EFAST and Sobol' methods and calibration of reduced state-variable TOMGRO model using genetic algorithms. *Comput. Electron Agric.* 100, 1–12. <https://doi.org/10.1016/j.compag.2013.10.006>.
- Wagner, M.P., Slawig, T., Taravat, A., Oppelt, N., 2020. Remote sensing data assimilation in dynamic crop models using particle swarm optimization. *ISPRS Int J. Geoinf.* 9 <https://doi.org/10.3390/ijgi9020105>.
- Wale, A., Dessie, M., Kendie, H., 2022. Evaluating the performance of aquacrop model for potato production under deficit irrigation. *Air, Soil Water Res.* 15 <https://doi.org/10.1177/11786221221108216>.
- Wang, G., Mehmood, F., Zain, M., Hamani, A.K.M., Xue, J., Gao, Y., Duan, A., 2022. AquaCrop model evaluation for winter wheat under different irrigation management strategies: a case study on the North China Plain. *Agronomy* 12. <https://doi.org/10.3390/agronomy12123184>.
- Wellens, J., Raes, D., Fereres, E., Diels, J., Coppys, C., Adele, J.G., Ezui, K.S.G., Becerra, L.A., Selvaraj, M.G., Dercon, G., Heng, L.K., 2022. Calibration and validation of the FAO AquaCrop water productivity model for cassava (*Manihot esculenta* Crantz). *Agric. Water Manag.* 263. <https://doi.org/10.1016/j.agwat.2022.107491>.
- Xing, H. min, Xu, X. gang, Li, Z. hai, Chen, Y. jin, Feng, H. kuan, Yang, G. jun, Chen, Z. xia, 2017a. Global sensitivity analysis of the AquaCrop model for winter wheat under different water treatments based on the extended Fourier amplitude sensitivity test. *J. Integr. Agric.* 16, 2444–2458. [https://doi.org/10.1016/S2095-3119\(16\)61626-X](https://doi.org/10.1016/S2095-3119(16)61626-X).
- Xu, C., Gertner, G., 2011. Understanding and comparisons of different sampling approaches for the fourier amplitudes sensitivity test (FAST). *Comput. Stat. Data Anal.* 55, 184–198. <https://doi.org/10.1016/j.csda.2010.06.028>.
- Xu, G., Yu, G., 2018. On convergence analysis of particle swarm optimization algorithm. *J. Comput. Appl. Math.* 333, 65–73. <https://doi.org/10.1016/j.cam.2017.10.026>.
- Yang, H., Yang, X., Heskell, M., Sun, S., Tang, J., 2017. Seasonal variations of leaf and canopy properties tracked by ground-based NDVI imagery in a temperate forest. *Sci. Rep.* 7 <https://doi.org/10.1038/s41598-017-01260-y>.
- Yue, J., Yang, G., Li, C., Li, Z., Wang, Y., Feng, H., Xu, B., 2017. Estimation of winter wheat above-ground biomass using unmanned aerial vehicle-based snapshot hyperspectral sensor and crop height improved models. *Remote Sens. (Basel)* 9. <https://doi.org/10.3390/rs9070708>.
- Zhang, Y., Walker, J.P., Pauwels, V.R.N., 2022a. Assimilation of wheat and soil states for improved yield prediction: the APSIM-EnKF framework. *Agric. Syst.* 201 <https://doi.org/10.1016/j.agsy.2022.103456>.
- Zhang, Y., Walker, J.P., Pauwels, V.R.N., Sadeh, Y., 2022b. Assimilation of wheat and soil states into the apsim-wheat crop model: a case study. *Remote Sens. (Basel)* 14. <https://doi.org/10.3390/rs14010065>.
- Zou, X., Möttus, M., 2017. Sensitivity of common vegetation indices to the canopy structure of field crops. *Remote Sens.* 9 <https://doi.org/10.3390/rs9100994>.